State representation of non-sensory neurons in visual cortical areas in the rat

A dissertation

submitted to the committee on graduate school of Brain Science, Doshisha university,

2022

In partial fulfillment of the requirements for the degree of Doctor of Science

Yuma Osako

Graduate School of Brain Science, Doshisha University

March. 2022

Abstract

It is widely assumed that trial-by-trial variability in visual detection performance is explained by the fidelity of visual responses in visual cortical areas influenced by fluctuations of internal states, such as vigilance and behavioral history. However, it is not clear which neuronal ensembles represent such different internal states. Here, I utilized a visual detection task, which distinguishes internal states in response to identical stimuli, while recording neurons simultaneously from the primary visual cortex (V1) and the posterior parietal cortex (PPC). I found that rats sometimes withheld their responses to visual stimuli despite the robust presence of visual responses in V1. My unsupervised analysis revealed distinct population dynamics segregating hit responses from misses, orthogonally embedded to visual response dynamics in both V1 and PPC. Heterogeneous non-sensory neurons in V1 and PPC significantly contributed to population-level encoding accompanied with the modulation of noise correlation only in V1. These results highlight the non-trivial contributions of non-sensory neurons in V1 and PPC for population-level computations that reflect the animals' internal states to drive behavioral responses to visual stimuli.

Acknowledgements

I am deeply indebted to a great number of people who made my thesis possible and who made my scientific experience in graduate school at Doshisha university an unforgettable time of studying and personal growth. I also acknowledge the people, both personal friends and family, for great supports to my student and research life at any given moment.

First, I am very indebted to my thesis advisor, Professor Yoshio Sakurai and Dr. Junya Hirokawa, who has been a wonderful, powerful, and thoughtful mentor and support for my study and college life for over six years. Their sincere instruction, sharp intellect, and persistent encouragement were all crucial to my achievement of this thesis research and my growth as a scientist. I feel that nothing could replace my experience in these years. I would also like to thank Sakurai laboratory members and the other laboratory professors in my graduate school: Tomoya Ohnuki, Kazuki Shiotani, Yuta Tanisumi, Hiroyuki Manabe, Eriko Ishihara, Shogo Takamiya, Prof. Susumu Takahashi, Prof. Jun Motoyama, Prof. Hiroaki Misonou, Prof. Takeshi Sakaba. They always supported me to make my research and my scientific mind sophisticated through serious discussion,

critical feedback to my thought, sharing a large number of scientific knowledge. And there are many other people whom I had the privilege of learning from Kohta I.Kobayasi, Yuta Tamai, Yuki Ito, Shota Murai, Shoko Yuki. There is no doubt in my mind that they have been a great servant of my growth as a scientist.

There are five friends to whom I express my deep gratitude: Yoshihito Saito, Masanori Kawabata, Ryosuke Takeuchi, Yusuke Atsumi, Gaku Hatanaka. I met them in my early graduate student at the conference and at the visit to their laboratories, and I now consider each of them closer as if I have been close friends from very early in our life. They always gave me critical advice, scientific knowledge, motivation, enthusiasm, and an encouraging voice for my research. They are always devoted to making research better and innovative and are passionate to elucidate the mechanisms of our brain from various perspectives. I was constantly surprised by their well-considered questions, solutions, and comments on the scientific problems. With these their mind, I deeply respect them as scientists and friends. Great encounters with them were all essential to the achievement of my research and my development as a scientist.

I also appreciate my thesis committee members: Prof. Susumu Takahashi, Prof.

Table of Contents

List of figures

1.   General introduction

One of the fundamental functions of the brain system is to use the external sensory input to make adaptive decisions about future behavior. Over the course of daily life, for instance, when the traffic light changes from red to green, we decide to 'go' action by our car. Behind this seemingly simple perceptual decision, our brains process the specific external information (the color of traffic light) and choose one action (go) among a set of multiple possible alternative actions. This decision is obviously influenced by sensory information. However, if the external sensory information is uncertain, our decisions might be fluctuated based not only on the external stimulus but also on a myriad of our internal factors (bias, fatigue, satiety, motivation, attention, etc., see Appendix 7.1). For example, in a foggy intersection, the attentive drivers may not initiate the 'go' action quickly, even if the traffic light turns from red to green. This is due to the driver's cautious anticipation of a traffic accident blunting his or her decision to guide the 'go' decision. These influences by the non-sensory internal factors to our decision can allow one to generate adaptive behavioral strategies in the various environments, and, together, they define an "internal state." (O'Doherty et al., 2004; Sugrue et al., 2004; Soltani and Koechlin, 2022).

It has been speculated that the sensory cortex is necessary for the sequence from processing the external sensory stimuli to decision making (Hubel and Wiesel, 1962; Gold and Shadlen, 2007; Glickfeld et al., 2013; Ibos and Freedman, 2017; Licata et al., 2017; Najafi et al., 2020; Goldbach et al., 2021). The visual cortex is believed to play a causal role in visually guided decision-making (Montijn et al., 2014; Licata et al., 2017; Jasper et al., 2019; Zhong et al., 2019). However, how the neuronal activities in the visual cortical area contribute to visually guided decision-making is yet largely unsolved.

Numerous studies have reported that the neurons in the visual cortex selectively fire to the visual stimulus features (Somers et al., 1995; Lampl et al., 2001; Lauritzen and Miller, 2003; Monier et al., 2003; Cardin et al., 2007; Schiller, 2010). In particular, the primary visual cortex (V1), which is the principal telencephalic recipient of visual input in primates and rodents, has historically been most studied. Hubel and Wiesel recorded the neuronal activity from the V1 and found a selective response to the specific tilts and direction of the visual stimulus (Hubel and Wiesel, 1959, 1962, 1963, 1974). Recent studies have shown that V1 neurons represent not only visual information but also a variety of non-visual features; Niell and Stryker found that the V1 shows more than a twofold increase of the visual responses during locomotion compared to stationary,

while the firing rates in the thalamus (lateral geniculate nucleus) did not increase with

locomotion (Niell and Stryker, 2010). They also found that specific narrow-spiking

neurons (see Appendix 7.2) are activated during running but suppressed by the visual

stimulus. Shuler and Bear reported that V1 neurons, which is solely selective to the

physical attributes of the visual stimuli, predict the accurate reward timing after visual-

reward association learning (Shuler and Bear, 2006; Monk et al., 2020). The other

studies revealed that V1 neurons show the mismatch responses strongly driven by

mismatch between predicted and actual visual feedback (Keller et al., 2012), the relative

value between multiple stimuli (Stănişor et al., 2013), and decision-related activity

(Nienborg and Cumming, 2014). These pioneering works imply that V1 neurons do not

function as only simple feature detectors but also reflect the non-sensory information

including animal's internal state. Furthermore, the posterior parietal cortex (PPC),

which is believed to be a part of the visual cortical area, was traditionally viewed as

being involved in visually guided decision making. A growing number of studies

(Shadlen and Newsome, 1996; Platt and Glimcher, 1999; Freedman and Assad, 2006;

Swaminathan and Freedman, 2012; de Lafuente et al., 2015; Goard et al., 2016)

revealed that the neuronal activity in PPC correlates with sensory-guided decisions. The

PPC represents not only sensory information but also motor-preparatory signals (Schall,

2001; Pho et al., 2018; Steinmetz et al., 2019), leading to speculation that PPC is involved in the decision process of the sensory to motor transformation. Direct inhibition of neuronal activity in the PPC impairs the motor aspects of decisions (Zhou and Freedman, 2019) (deciding where to move), evidence accumulated decision which restricted to the visual than auditory task (Licata et al., 2017), visual memory guided decision (Goard et al., 2016) (deciding action based on the memory), and virtual navigation decision (Harvey et al., 2012; Driscoll et al., 2017) (deciding action based on the cue in the virtual navigation environment) indicating that the PPC plays a causal role more specific in visually guided decision making. Furthermore, PPC neurons represent the history-dependent bias (Morcos and Harvey, 2016; Hwang et al., 2017, 2019; Hattori et al., 2019) and task- and context-dependent sensory signals (Gail and Andersen, 2006; Pho et al., 2018). These findings lead the speculation that the PPC is involved in the decision making coupled with the sensory signals and internal states (e.g., reward bias and motivation). However, how internal factors are represented in the visual cortical areas and coded with sensory information simultaneously is still enigmatic.

Studying the neuronal activity underlying visually guided decision behavior, however, requires careful psychophysical readouts that constrain task design. In

previous studies, visual detection tasks, in which subjects report whether or not a visual

stimulus is presented, have historically been introduced to quantify the decision making.

In particular, most of the task applied the Go/Nogo paradigm, in which subjects perform

a specific action (e.g., pull a lever) when they detected a certain stimulus (Go action),

while they are instructed to inhibit their habitual go action (e.g., still) if the stimulus was

omitted (Nogo action). This paradigm is the simplest cognitive task to explore the brain

mechanisms underlying inhibitory control, action selection, and more widely, cognitive

control (Criaud and Boulinguez, 2013). However, the Go/Nogo task contains the

problem that it cannot guarantee that the animals failed to detect the visual stimulus in

the Nogo trials. The Nogo trials contain the following two distinct cognitive stages.

First, animals actively suppress overt Go action based on visual perception. Second,

they actually perceive the stimulus, but it was not substantial evidence to drive the Go

action during the response timing. The difference between these two behavioral

performances is whether they actually perceived the stimulus or not. Unless care is

taken to explicitly control for this confound, a nontrivial misunderstanding of the

neuronal mechanism of decision making may be drawn in comparison between

Go/Nogo actions and neuronal activity. This potential confound is especially important

because many of the visual cortical areas identified as playing a role in decision making

have also been implicated in visual perception. Regarding this background, it is

essential to design the quantitative task to distinguish the different Nogo actions.

2.   A novel perceptual decision-making task in rats

2.1 Summary

To study visually guided decision in the animals, appropriate method evaluating the

decisions based on the perceptual judgement is required as described in the general

introduction. In this section, I established a novel behavioral task for rats to test their

spatial-visual cue detection ability, using a two alternative choice (2-AFC) task with and

without a third choice option where animals get rewards only in the objective absence of

a visual cue. In the trials without the third option, spatial choice accuracy decreased

from near perfect to near chance levels as the visual cue brightness decreased. In

contrast, with the third option, the rats exhibited >90% spatial choice accuracy

regardless of the cue brightness. The rats chose the third choice option less frequently

when the cue was brighter, suggesting that rats have a generalized strategy to make

spatial choices only when their internal detection criterion is met. Interestingly, even

when the animals chose the third option, they could still significantly and correctly

choose the direction of the visual stimuli if they were forced. My data suggest that the

rats' variable detection performance with identical set of stimuli is derived from

stochastic processing of visual signals with a certain internal detection threshold rather than general motivational threshold.

2.2 Introduction

Subjective perception is often contrasted with objective perceptual performance (Kim and Blake, 2005; Kanai et al., 2010; Dehaene and Changeux, 2011), suggesting that perceptual awareness is not always an accurate monitoring process of one's own capability. A striking example of this distinction is patients with damage to their primary visual cortex (V1) who have the capacity to detect or discriminate visual stimuli without conscious perception (Campion, 1983; Weiskrantz, 1986; Tong, 2003). This phenomenon is called "blindsight," and the dissociation between conscious perception and behavioral performance suggests that humans process visual information without subjective visual awareness. Macaque monkeys with unilateral V1 lesions perform similarly to human blindsight subjects in various behavioral tasks (Humphrey, 1974; Cowey and Stoerig, 1995; Christopher and Sean, 2006; Yoshida et al., 2008, 2012, 2017; Yoshida and Isa, 2015), suggesting the generality of the phenomenon across species. Clarifying the neural correlates of dissociation between subjective visibility and objective behavioral performance is key to understanding the neural mechanisms of

8

generating metacognition and consciousness (Ress et al., 2000; Goebel et al., 2001; Stoerig et al., 2002; Peter et al., 2005; Soma et al., 2014). To this end, establishing a rodent model for quantitative evaluation of dissociation between subjective and forced performances would be useful for extending research to the molecular and neural circuit levels.

Recent behavioral studies have provided evidence for metacognition in rats (Foote and Crystal, 2007, 2012; Yuki and Okanoya, 2017). Foote and Crystal set up two types of trials in which rats could decline the test (choice trial) or were forced to take the test (forced trial) in a sound duration–discrimination task. Because rats in the choice trials could only take the test when they were confident of a correct choice, the accuracy in these trials was greater than in the forced trials. Indeed, the proportion of rats that declined the test in the choice trials increased with increasing difficulty of discrimination. They concluded that rats had the capacity to use their internal state for behavioral performance, which could be called metacognition. Kepecs et al. established a theoretical framework for estimating the degree of metacognition (i.e., decision confidence), and proposed a trial-by-trial instantaneous measurement of decision confidence in an odor mixture categorization task in rats (Kepecs et al., 2008; Kepecs and Mainen, 2012; Lak et al., 2014; Hangya et al., 2016). These studies demonstrated

the strength of quantitative measurement of metacognition for clarifying the neural

correlates of such internal variables (Kepecs et al., 2008; Hirokawa et al., 2019).

Although post-decision wagering – such as the waiting time paradigm – is useful for

measuring metacognition as a quantitative variable (Persaud et al., 2007; Persaud and

McLeod, 2008), awareness itself can be a binary phenomenon (Overgaard et al., 2006;

Del Cul et al., 2007). The subjective presence of perception, i.e., awareness, is

dynamically influenced in an all-or-nothing manner by experimental manipulations such

as top-down attention (Koch and Ullman, 1985; Newby and Rock, 1998; Kanai et al.,

2006, 2008; Watanabe et al., 2011), multisensory integration (Geldard and Sherrick,

1972; McGurk and MacDonald, 1976; Shams et al., 2002) and inter-hemispheric

interactions (Walker and Powell, 1979; Blake and Logothetis, 2002; Tsuchiya and Koch,

2005) despite the continuous physical presence of stimuli. This implies separable neural

substrates of awareness and decision confidence. However, in rodents, it is not known

whether they have an internal detection criterion dissociated from forced performance.

In our previous studies using rats, we showed that visual detection performance is

modulated by the animals' internal states, such as top-down attention and multisensory

integration (Sakata et al., 2002, 2004; Hirokawa et al., 2008, 2011). These studies raised

the question of whether rats could reliably utilize internal visual information. To clarify

whether rats have internal criterion-based visual detections dissociated from criterion-independent visual detections, I compared the detectability of identical sets of spatial visual stimuli with and without a third choice option, which affords animals the opportunity to report the subjective absence of a visual cue. Note that animals were rewarded by choosing the third choice option only when the visual cue was not actually emitted. Therefore, optimal strategy in this task is to make the peripheral choice as long as the rats detected a peripheral visual cue regardless of the availability of the third choice option.

2.3 Experimental procedures

Subjects

Five male Long–Evans rats (Shimizu Laboratory Supplies, Kyoto, Japan) aged 12–17 weeks and weighing 250–500 g at the beginning of the training were individually housed under standard laboratory conditions in a light and dark cycle (lights on at 8:00 and off at 21:00) with food freely available. The rats were placed on a liquid restriction schedule with daily body weight monitoring to ensure that body mass remained within 85% of prior mass before restriction. The rats received water during each behavioral session and ad libitum in the 10 min after the session in their home cage. Two out of

11

five rats were excluded from analysis because they could not achieve the training

criterion in 3-choice training phase within our limited time. All experiments were

performed in accordance with the guidelines for animal experiments at Doshisha

University with the approval of the Animal Research Committee of Doshisha

University.

Apparatus

The behavioral apparatus was assembled based on the previous works (Hirokawa et

al., 2011) with modifications for the water reward using Bpod and PulsePal (Sanworks

LLC, NY, USA)(Sanders and Kepecs, 2014), which are open source TTL event

measurement and control devices designed for behavioral tasks. My system comprises

identical operant chambers (O'Hara & Co., Tokyo, Japan), each located in a soundproof

box (Brain Science Idea Co. Ltd., Osaka, Japan), with three nose poke ports in the front

wall and a shutter door for the central port. The three ports were equipped with interior

illumination (white light-emitting diode (LED)) and infrared photodiodes, and

interruption of the infrared beam signaled port entry with a TTL pulse. A water reward

could be delivered from the gravity-fed reservoirs, which were regulated by solenoid

valves (The Lee Company, CT, USA). The reward amount, which was determined by

the solenoid valve opening duration, was set to 0.01 ml and regularly calibrated. The

shutter door for the central port was controlled by Arduino Due (Italy). Visual stimuli

were presented on either the left or right side where the rats' eyes were directed when

they poked the central port (Hirokawa et al., 2011). The visual stimulus was a white

LED (4000 mcd; RS components, Japan) covered by a frosted plastic diffuser to

generate homogenous illumination.

Visual cue detection task

The task design was based on the previous study (Hirokawa et al., 2011), with

modification of the free choice and FC paradigms from (Foote and Crystal, 2007). The

task was comprised of randomly interleaved three choice (3C) and forced-choice (FC)

trials with equal probabilities in a session. The only difference between the trial types

was that, in FC trials, the central port was shut with the shutter door to prevent the rat

from continuing to central nose poke (Fig. 1). After a fixed 2.5 s inter-trial interval (ITI),

the central port was illuminated by an interior LED of the central port signaling the

ready state of a trial initiation. The rats initiated each trial by making nose pokes into

the central port. After a 0.2–0.6 s random stimulus delay, the visual stimulus was

presented from the left or right side for a duration of 0.2 s. Rats were allowed to make a

choice response after the end of the stimulus delay period. The trials where animals

prematurely left the port before stimulus delay were canceled and they needed to re-

initiate the trials. I randomly provided one of three levels of visual brightness (difficult,

normal, and easy) for each trial by modulating the voltage ranging 0.02–5.1 lx. Difficult,

normal and easy stimuli were selected for each subject such that the subject detected the

stimuli with respective accuracy of 55%–65%, 65–80% and >80%, respectively, in the

forced-choice (FC) trials. The probabilities for left, right, or no visual stimulus were

equal (33% per condition) in 3C and FC trials (Fig. 1A-B). The reward was given if rats

chose the same side where the visual stimuli was emitted in the 3C and FC trials. If

animals kept nose poke more than X s in the central port after the presentation of the

visual stimuli, the trial was treated as miss error. X were drawn from the uniform

distribution with a range of [0.5, 1]. Note that X is aligned with the expected timing of

the reward delivery in no-signal trials so that animals cannot utilize the absence of

reward delivery as indication of the presence of unnoticed visual stimuli. Failure of the

peripheral choices within 5 s after nose withdrawal from the central port was also

treated as miss error, though it occurred rarely (<5%). There was no punishment in any

error trials and next trial was allowed to be initiated after ITI. In the no-signal trials,

animals need to wait for 0.2–0.6 s without stimulus and another 0.5–1 s to get reward

from the central port. There was no cue to distinguish the initial delay (0.2–0.6 s) and

reward delay (0.5–1 s). Thus, animals did not have any external clue to differentiate the

signal trials from the no-signal trials, except for the presentation of the signal itself. In

the FC trials, the shutter was closed 0.5 s~ after stimulus presentation onset, and the rats

were forced to choose either the left or right port (Fig. 1A-B, Forced choice). In cases

where no stimuli were presented in FC trials, the animals were never rewarded. After

task training (see below in details) was complete, the visual detection task was tested for

10 sessions for each rat. Each session was terminated when the rats completed more

than 500 trials, which usually takes 2 hours.

Training procedure

Initial training

On the first day of training, rats were acclimated to the operant chamber. A water

reward was given in the central port illuminated by an interior LED light. On the

following day, the interior LEDs for the left and right ports were illuminated 0.1 s after

the center poke in, and nose poke into those peripheral ports was immediately rewarded

in the same port. The initial delay for illumination of the peripheral ports was extended

from 0.2 to 0.6 s over the subsequent 2–4 days. The initial training phase conditioned

the animals to poke the central port to initiate the trial (initial poke) and make a

subsequent peripheral nose poke into the left or right port.

3-choice training

In the next step, the peripheral visual stimulus was presented using either the left or

right LED apparatus for 0.2 s. Animals were rewarded if they poked their nose into the

peripheral port on the same side as the visual stimulus. Once choice accuracy exceeded

the criterion (>90%), the interior LEDs were turned off except for the LED in the

central port. In the next step of this training phase, the peripheral visual stimuli were not

presented and the rats were trained to maintain a central nose poke for 0.5–1.0 s for

15 µl of water reward. In the last step, left, right, or no visual stimulus was presented

with equal probability (33% per condition) in a pseudorandom order and animals were

rewarded for making a left, right, or central choice, respectively. This procedure lasted

10–20 days to meet the criterion (Choice accuracy >90% and the central poking

accuracy >90%).

Forced-choice training

In the next step of visual detection task training, FC trials were introduced. When the rats poked into the central port to initiate the trial, the shutter closed the central port 0.5 s after stimulus presentation. Once the shutter closed the central port, the rats were forced to nose poke either the left or right port since they could not maintain the central poke. No reward was given when the visual stimulus was not presented in FC trials. When the animals met the criterion of 80% choice accuracy, they advanced to the last stage of visual detection task training. This procedure lasted 5–10 days to meet the above criterion.

Mixed-choice training

In the final step of visual detection task training, both 3-choice and forced-choice trials were interleaved in a single session. Once animals achieved 90% accuracy in 3-choice trials and more than 80% accuracy in forced-choice trials, we introduced three grades of visual stimuli difficulty using different brightness levels. The brightness was modulated to be easy, normal, or difficult, as described above. This training lasted 10–20 days.

Behavioral data analysis

All statistical analysis of behavioral data was conducted using MATLAB 2017a

(Mathworks). Hit, miss, and false alarm rates were defined in 3C trials. The miss rate

was the percentage of central port choices in trials where visual stimuli were presented;

the hit rate was the percentage of peripheral port choices where visual stimuli were

presented, regardless of the correctness of the choice side; and the false alarm was the

percentage of peripheral port choices in trials where no visual stimuli were presented.

Reaction time was defined as the duration from stimulus presentation onset to nose

withdrawal from the central hole. Trials with a reaction time of less than 130 ms was

considered as invalid, which correspond to $2.75 \pm 0.8\%$ of the total number of trials,

were excluded from the calculation of the spatial choice accuracy as they were too early

to have been responses to the stimulus (Histed et al., 2012). For the analysis of data

across the conditions, one-way ANOVA and Tukey's test for post-hoc comparison were

used. For analyzing the choice accuracy after shutter release in the FC trials (Fig. 5), the

student's t-test was used to compare chance levels ($p = 0.5$). All data are presented as

mean $\pm$ SEM.

2.4 Results

Comparison between 3C and FC trials

The rats initiated each trial by making nose pokes into the central port and the visual stimulus was presented (or not presented) from the left or right side after a 0.2–0.6 s random delay (Fig. 1A-B). The task was comprised of randomly interleaved three choice (3C) and forced-choice (FC) trials with equal probabilities in a session. The only difference between the trial types was that, in FC trials, the central port was shut 0.5 s after the stimulus presentation timing with the shutter door to prevent the rat from continuing to central nose poke (Fig. 1).

The choice accuracy in FC trials decreased from approximately 90% to 65% as the visual brightness decreased (Fig. 2A–C). By contrast, the choice accuracy was maintained at >90% regardless of the decrease in visual brightness in the 3C trials (Fig. 2A–C), while the rats missed the visual stimuli more often (from 20% to 80%) as the visual brightness decreased (Fig. 2D–F). The false alarm rate in the 3C trials was less than 5% on average (mean $\pm$ SEM: 3.69% $\pm$ 0.89 (n = 3)) when the visual stimulus was not presented. These results indicate that the hit rate in 3C trials reflects the probability that the rats recognized the visual cue.

Reaction time between 3C and FC trials

To understand detection performance relative to the shutter closure timing, the

reaction times of the behavioral responses in the 3C and FC trials were analyzed along

with detection accuracy. In 3C trials, the reaction times for correct choices have a sharp

peak at around 0.2 s (Fig. 3), showing that highly stereotypic responses to visual stimuli

are repeated when the rats make correct choices. The reaction time distribution was

slightly shifted to earlier time points in easier trials. By contrast, reaction times in

erroneous trials were scattered without a specific peak, suggesting that incorrect choices

were made at random without a specific clue. The choice accuracy in the 3C trials

reached 100% at around 0.2 s and was maintained near 100% by at least 0.5 s (Fig. 3.

Upper, rat 1 and rat 2), whereas a prolonged tail of reaction time distribution (up to 1 s)

was observed in rat3. Overall, more than 95% of correct-responses were made before

0.5 s in 3C (rat1: 97.89%, rat2: 97.12%, rat3: 96.25%, Table 1 in detail). As expected,

there were no significant differences between the 3C and FC trials before the expected

time for the shutter closure for each stimulus condition ($p > 0.05$, Kolmogorov-Smirnov

test, Fig. 3 and Fig. 4). The reaction time analysis shows that the degraded accuracy in

FC trials is mostly derived from the forced choices after the shutter closure.

Detection accuracy after the shutter closure

Next, we examined whether the forced choice after the shutter closure was by chance (50%) or above chance. Surprisingly, the rats still significantly chose the correct side in a visual difficulty-dependent manner; All three rats significantly chose the correct side in easy and normal conditions (Fig. 5, t-test from chance level); one animal (rat 3) performed above chance level in the difficult condition, while the others (rat 1 and rat 2) performed at the chance level in the difficult condition (Fig. 5). In addition, the proportion of correct choices after 0.5 s of the stimulus onset in FC was much larger than those in 3C (insets in Figs 3 and 4), suggesting that the residual accuracy after the shutter closure in FC is not explained by the correct choices with slow reaction time observed in 3C. These results suggest that the animals sometimes failed to make hit-responses even though they could choose the correct side if forced. We note that there is a weak trend of the decrease in choice accuracy before the shutter closure in FC in difficult trials (compare accuracies before the shutter closure in Fig. 5 and those in 3C in Fig. 2). However, the direct comparison between the accuracies between 3C and FC before the shutter closure were not significant ($p > 0.05$, one-way ANOVA and Tukey's test for post-hoc comparison), except for one animal (rat1: $p = 0.03$ in difficult trials), suggesting the effect is due to subtle experimental fluctuation. We then asked if the failure of the hit-response before the shutter closure in eventually-correct trials was due

to general procrastination (including longer reaction time) or degraded visibility. If the former is the case, failed hit-responses should occur independently of the visual difficulty, and therefore the ratio of correct responses after the shutter closure relative to all correct responses should be constant across visual difficulty levels. Our data did not support this possibility. Instead, failed hit-responses significantly decreased with increasing visual difficulty (analyzed in a one-way ANOVA for each visual difficulty level and a post-hoc test adjusted for multiple comparisons), supporting the notion that animals stayed in the central port by the time the shutter closes due to degraded visibility.

2.5 Discussion

In this chapter, I developed a behavioral paradigm for rats to detect spatial visual cues with graded brightness and then examined how their detection performance with and without a third choice option were dissociated. My results demonstrated that rats have a generalized criterion in reliably detecting visual stimuli with different luminance and that it cannot be explained by general motivational threshold, arguing for the presence of visual awareness in rats. The results are generally consistent with previous findings in the sense that rats can utilize their internal state for subsequent decision-

making (Foote and Crystal, 2007; Kepecs et al., 2008; Yuki and Okanoya, 2017). My behavioral task was also designed to be compatible with multiunit recordings and optogenetics with a complete experiment for each session with multiple randomly interleaved conditions, which is potentially useful in the search for neural correlates of visual awareness and visually guided decision making.

Previous studies have demonstrated that rats have the ability to utilize decision confidence in sound (Foote and Crystal, 2007) and odor categorization (Kepecs et al., 2008; Lak et al., 2014) tasks. However, a perceptual categorization task does not guarantee categorically distinct awareness because the decision boundary for the categorization is arbitrarily set by the experimenters regardless of the rats' subjective perception. In addition, uncertain responses owing to "intermediate" stimuli are often confounded by reinforcement or economic strategies without requiring metacognition (Jozefowiez et al., 2009; Brown et al., 2017; Templer et al., 2017). In this study, we utilized a binary visual detection task where such "intermediate" cues were not available: rats were rewarded in peripheral ports when visual stimuli were actually emitted from either the left or right side, or they were rewarded in the central port when visual stimuli were not emitted. Thus, there was no ambiguity in stimulus-reward association unlike in the sensory categorization task described above. Indeed, the spatial

choice accuracy was consistently >90% regardless of the visual brightness in shorter

reaction time trials (<0.5 s), whereas the overall accuracy decreased to 60% in low

visual brightness in the FC trials (Figs 2, 3 and 4). This suggests that rats have a

generalized strategy to choose the peripheral ports when their internal detection

criterion is met.

It has been shown that the difference in the performance between a yes-no detection

task and a forced choice task disappears in human subjects when considering decision

bias (with some exceptions such as the "blindsight" cases). Therefore, one may argue

that the difference in accuracy between 3C and FC in our task may be also explained by

decision bias rather than detectability difference. Consistent with this idea, our data

suggest that the difference is mainly from conservative decision criterion in 3C.

Because the 3C and FC are essentially indistinguishable for animals until the shutter

closure as designed, the discriminability and the bias should be also same between 3C

and FC at least by the time of 0.5 s after the stimulus onset. Therefore, the high accuracy

in 3C reflect the above-criterion choice whereas the degraded choice accuracy in FC is

sub-threshold forced choice. Though we observed a weak decrease of choice accuracy

in difficult trials before the shutter closure in FC (Fig. 5), the significant effect was only

found in one animal, likely due to a subtle conditional fluctuation such as unreliable

mechanical onset of the shutter closure. We think the effect (~5%) is negligible

considering the large dissociation of the accuracy (~35%) observed in 3C and FC (Fig.

2). In addition, it is unlikely that the minor decrease of the accuracy contributes to the

increased accuracy after the shutter closure (Fig. 6). Therefore, I conclude that the

difference in spatial accuracy in FC and 3C is simply derived from the conservative

detection criterion in 3C.

Though signal detection theory provides one of the solutions to disambiguate the

effect of detectability and the response criterion in an objective way (Meier and

Reinagel, 2011; Carandini and Churchland, 2013), it is hard to apply signal detection

theory directly to our dataset because of the complexity of our task design. One

drawback to applying signal detection theory to the study of awareness in animals is

that it requires the experimenters to obtain multiple data points with different decision

criteria. As a result, the animals might adaptively adjust their decision criterion based on

their motivational state and therefore their subjective report may no longer reflect their

sensory awareness. In this behavioral study, I trained animals to minimize their false

alarm rates (i.e., go response without signal) by reinforcing them to maintain a central

poke as the default state. As a result, I obtained reliable go-responses with high

discrimination accuracy (~95%, Fig. 2) regardless of the stimulus intensity and a low

false alarm rate (<5%), demonstrating that rats are capable of a highly reliable

subjective report of their visual detection across different signal levels.

While animals could choose the correct side with near perfect accuracy (>90%)

when they made a hit-response, they missed the same stimuli so often, especially for

low brightness (60–80%). What causes this response variability? In my behavioral task

setting, the animals maintained their heads in the central port while the visual stimuli

were delivered from identical peripheral positions. Therefore, one possibility is that the

missed trials may be due to decreased visual signals given a conservative threshold due

to the animals' fluctuating internal states (e.g., visibility, confidence) and/or physical

changes in light reception on their retina. The alternative possibility is that it is due to a

general conservativeness or bias to the central port unrelated to signal levels. To

discriminate between these possibilities, I introduced trials where the animals were

forced to choose the direction of the cue (i.e., FC trials) and analyzed a fraction of the

choices where animals failed to make hit-responses by the time of the shutter closure.

To our surprise, the rats could still make correct choices depending on the strength of

the visual stimuli (Fig. 5). Importantly, the occurrence of correct choices after the

shutter closure was not explained by randomly omitted/procrastinated hit-responses

(i.e., center bias), but rather was anti-correlated with stimulus intensity (Fig. 6). The

results indicate that the variable detection performance to identical stimuli is derived

from stochastic internal processing of visual signals with a certain internal threshold.

Whether or not such an internal threshold is related to the decision itself (e.g.,

payoff (Carandini and Churchland, 2013; Berditchevskaia et al., 2016), confidence

(Kepecs et al., 2008), expectation (Yoshida and Isa, 2015)) or to subjective visibility is

not directly demonstrated in our experiments. For instance, it has been shown that

frequent reward condition lowers the decision criterion of subjects, whereas difficult

task increases the decision criterion (Niv et al., 2007). Thus, animals may adjust their

decision criterion based on overall task difficulty rather than faithfully following their

vision. Note that such internal threshold is different from the fluctuation of general

motivation discussed (Fig. 6) because it depends on sensory evidence. In addition, it is

also possible that the optimal threshold was adjusted by the tradeoff between reward

values and the reward likelihood estimated trial-by-trial from internal visual signals

regardless of the visual awareness. It is possible to differentiate these possibilities by

systematically changing the center reward value and seeing how the spatial choice

accuracy and false alarm rates for 3C would change. However, we emphasize that

considering the fact that the rats were never rewarded by remaining in the central port in

the presence of stimuli and there is no objective ambiguity in the stimulus-reward

association, there is little room for trading between detection confidence and the center

reward value. Therefore, it is more plausible that the threshold is related to visibility

rather than an adaptive decision criterion.

Compared with the dissociation reported by Foote & Crystals (2007), the extent of

dissociation in our study was larger and more robust (compare Fig. 2E,F, and G in Foote

& Crystals (2007) and Fig. 2 in this behavioral study). The reason for this discrepancy

can be largely explained by differences between awareness and confidence reports.

Confidence reports for categorization rely on the degree of difference in the competing

evidence, and the forced categorization may use the sign of the evidence. Therefore,

confidence reports and forced performance are unavoidably correlated with each other.

In contrast, awareness reports rely on the threshold of sensory evidence; subjects will

report otherwise as long as the sensory evidence does not reach the threshold. Once the

sensory evidence reaches the threshold, the report is reliable since it is supported by a

high degree of sensory evidence. Therefore, the dissociation will be large in the

perceptual awareness report task.

It is intriguing to consider what neural mechanisms enable above-threshold vision to

be dissociated from sub-threshold vision. It is advantageous to utilize rodents as model

animals given the number of molecular biology tools available. I also note that our

behavioral setup utilizes a commercial standard operant box with nose pokes and an

open-source behavioral control system, which is readily available to the community. On

the other hand, a disadvantage of the current protocol is the lack of precise control of

the visual stimuli on retina, which is a standard procedure in non-human primate

studies. Random presentations of visual stimuli on the retina would inevitably cause

random noise in the behavioral results, causing difficulty in the interpretation of neural

correlates of subjectivity. One way to overcome this issue is to utilize head-fixed

animals (Kimura et al., 2012), head-mounted goggles (Arens-Arad et al., 2016) or direct

activation of sensory neurons (Yang et al., 2008). Next section, I recorded neuronal

activities from the visual cortical area during this novel visual cue detection task.

3 Neural representation of internal states in the visual cortical area

3.1 Summary

It is widely assumed that trial-by-trial variability in visual detection performance is explained by the fidelity of visual responses in visual cortical areas influenced by fluctuations of internal states, such as vigilance and behavioral history. However, it is not clear which neuronal ensembles represent such different internal states. In this section, I utilized a visual detection task described in chapter 2, which distinguishes internal states in response to identical stimuli, while recording neurons simultaneously from the V1 and the PPC. I found that rats sometimes withheld their responses to visual stimuli despite the robust presence of visual responses in V1. My unsupervised analysis revealed distinct population dynamics segregating hit responses from misses, orthogonally embedded to visual response dynamics in both V1 and PPC. Heterogeneous non-sensory neurons in V1 and PPC significantly contributed to population-level encoding accompanied with the modulation of noise correlation only in V1. These results highlight the non-trivial contributions of non-sensory neurons in V1 and PPC for population-level computations that reflect the animals' internal states to drive behavioral responses to visual stimuli.

3.2 Introduction

Identical sensory stimuli sometimes evoke different perceptual and behavioral

responses. For instance, in a sensory detection task, human or animal subjects are

instructed or well trained to reliably report the presence or absence of sensory stimuli to

obtain rewards. When the sensory stimulus is near the threshold to prompt a decision,

subjects' responses vary across trials despite their best efforts to get the reward.

Interestingly, even if they report absence of stimuli, it is sometimes possible for them to

correctly guess above chance level if they are forced to answer (Kolb and Braun, 1995;

Merikle et al., 2001; van Vugt et al., 2018). Revealing the neuronal mechanisms

underlying such trial-by-trial variability of perceptual responses is crucial to understand

how the brain exploits sensory information for optimal decision making.

Trial-by-trial variance of responses to identical stimuli is believed to reflect noise in

the conversion of sensory information into motor outputs (Osborne et al., 2007). It has

been demonstrated that the variability of the firing rates of sensory neurons is

responsible for the variable response to different choices (Tolhurst et al., 1983; Parker

and Newsome, 1998). However, accumulating evidence suggests that perceptual

decisions are also significantly affected by latent subjective states reflecting task

engagement (Busse et al., 2011). For instance, behavioral response variability is correlated with mind wandering in humans (Smallwood and Schooler, 2006) and fluctuations of physiological and behavioral states in animals (Critchley and Rolls, n.d.; Aston-Jones and Cohen, 2005; Harris and Thiele, 2011; Schriver et al., 2018). These subjective state drifts could be partially attributed to cortical activity fluctuation (Monto et al., 2008; Niell and Stryker, 2010; Harris and Thiele, 2011). The synchronization and desynchronization of many neurons in particular areas of the cortex could affect the efficiency of population coding (Shimaoka et al., 2019; Jacobs et al., 2020). Accordingly, shared response variability in pairs of sensory neurons (i.e., noise correlation), modulated by attention, arousal, and reward expectation, can affect efficient coding of stimulus features and sensory processing, resulting in behavioral variability in a sensory detection task. Moreover, task engagement is known to be modulated by the trial-by-trial experience of decision making and varying outcomes (Daw et al., 2006; Gold et al., 2008; Akaishi et al., 2014; Fritsche et al., 2017; Lak et al., 2017, 2020; Fan et al., 2018), in turn regulated by distinct neuron populations in association areas (Hwang et al., 2017; Hirokawa et al., 2019; Masset et al., 2020). Furthermore, some studies have suggested that neurons that do not explicitly respond to a stimulus contribute to texture discrimination in the somatosensory cortex (Safaai et

al., 2013), working memory coding in the prefrontal cortex (Leavitt et al., 2017), stimulus/choice coding in the auditory cortex (Insanally et al., 2019), and category representation in the prefrontal cortex (Insanally et al., 2019). These studies highlight the potential contribution of non-sensory neurons to modulating sensory processing. However, how non-sensory neurons coordinate with sensory neurons to optimize sensory decisions is yet unknown.

Numerous studies have revealed that neuronal activity in the primary visual cortex (V1) and posterior parietal cortex (PPC) plays a crucial role in visual detection (Silvanto et al., 2009; Goard et al., 2016). Patients with V1 lesions reported subjective blindness (Campion, 1983; Weiskrantz, 1986), and direct optogenetic inhibition of rodent V1 impaired visual detection behavior (Glickfeld et al., 2013). On the other hand, the PPC is known to play essential roles in selective attention and reward-history bias (Hwang et al., 2017, 2019) and regulates the response properties of V1 neurons (Marques et al., 2018; Hishida et al., 2019; Keller et al., 2020). Recent imaging studies have examined visual perceptual behavior during a go or no-go detection task and found that task requirements (Pho et al., 2018) heavily modulate visual responses in the PPC and that heterogeneous recruitment of V1 neurons plays an important role in visual detection

(Montijn et al., 2015; Pho et al., 2018). Together, these studies support the notion that the V1 and PPC create distinct cortical states at the population level that integrate task-relevant external signals (Hanks et al., 2015) with internal states for subjective detection performance.

Although neuronal imaging studies addressed population coding of sensory processing across different cortical areas, the go or no-go task paradigm, often used in experiments with head-fixed animals, is susceptible to subjective biases: go trials may contain false alarms and no-go trials may contain misses (Green et al., 1966) due to fluctuating internal states, as described above. To further classify such internal states during visual detection, I developed a spatial-visual cue detection task for free-moving rats in chapter 2. The task combines a two-alternative spatial choice with a third option for no stimulus, which allowed us to isolate the hit trials less contaminated with false alarms. Furthermore, we utilize a shutter for the central port that enables us to force rats to make spatial choices, even when they initially chose the central port. It separates the miss responses into two distinct categories: "missed responses with the capability to choose the correct side when forced (Miss+)" and "missed responses without the capability to choose the correct side when forced (Miss−)." This allows us to uniquely

interrogate how visual information in the visual cortex fails to drive correct choice behaviors by comparing "self-driven correct choice" and Miss+ conditions. By taking advantage of these relatively homogeneous trials with different behavioral responses to identical stimuli, we aimed to reveal the neural mechanisms underlying variable visual detection performance due to subjective biases. We recorded neuronal activity simultaneously from V1 and PPC to test how sensory and non-sensory neurons (hereafter defined as "stimulus non-preferring neurons") in these cortical areas differently contribute to the population-level computation for visually guided decisions.

3.3 Experimental procedures

Subjects

Seven male Long-Evans rats (Shimizu Laboratory Supplies, Kyoto, Japan) weighing 200-268 g at the beginning of training were individually housed and maintained on a laboratory light/dark cycle (lights on 8:00 A.M. to 9:00 P.M.). Rats were placed on water restriction with ad libitum access to food. The animals were maintained at 80% of their baseline weight throughout the experiments. All experiments were implemented in accordance with the guidelines for the care and use of laboratory animals provided by the Animal Research Committee of Doshisha University.

Surgery

Rats were anesthetized with 2.5% isoflurane before surgery, and anesthesia

maintained throughout surgical procedures. I monitored body movements and hind leg

reflex and adjusted the depth of anesthesia as needed. An eye ointment was used to keep

the eyes moistened throughout the surgery. Subcutaneous scalp injection of a lidocaine

1% solution provided local anesthesia before the incision. A craniotomy was performed

over the anterior part of the right V1 (AP −6.36 to −7.32 mm, ML 3.2 mm relative to the

bregma, 0.2 to 0.4 mm below the brain surface), and right PPC (AP −3.8 mm, ML: 2.5

mm relative to the bregma, 0.2 to 0.4 mm below the brain surface), and a custom-

designed electrode was vertically implanted using a stereotactic manipulator. A

stainless-steel screw was placed over the cerebellum and served as ground during

recordings. The mean response of all electrodes was used as a reference. During a week

of postsurgical recovery, I gradually lowered the tetrodes to detect unit activities in the

V1 and PPC. Electrode placement was estimated based on depth and was histologically

confirmed at the end of experiments.

Histology

Once the experiments were completed, the rats were deeply anesthetized with

sodium pentobarbital and then transcardially perfused with phosphate-buffered saline

and 4% paraformaldehyde. The brains were removed and post-fixed in 4%

paraformaldehyde, and 100 μm coronal brain sections were prepared to confirm the

recording sites (Figure 7).

Behavioral apparatus

The behavioral apparatus has been previously described (Osako et al., 2018; Ohnuki

et al., 2020). An operant chamber (O'Hara, Tokyo, Japan) with three ports in the front

wall for nose-poke responses was enclosed in a soundproof box (Brain Science Idea,

Osaka, Japan). Each port was equipped with an infrared sensor to detect the animals'

nose-poke responses. Visual cues were presented using white light-emitting diodes

(LEDs) (4000 mcd; RS Components, Yokohama, Japan) placed on the left and right

walls of the operant chamber, as shown in Figure 1. Water rewards were delivered from

gravity-fed reservoirs regulated by solenoid valves (The Lee Company, Westbrook, CT)

through stainless tubes placed inside the central, left and right target ports. Stimulus and

reward deliveries were controlled with Pulse Pal(Sanders and Kepecs, 2014) and

behavioral responses measured using Bpod (Sanworks, Stony Brook, NY).

Visual cue detection task

The task design was based on (Hirokawa et al., 2011), with modification of the free

choice and FC paradigms from (Foote and Crystal, 2007). The task was comprised of

randomly interleaved three choice (3C) and forced-choice (FC) trials with equal

probabilities in a session. The only difference between the trial types was that, in FC

trials, the central port was shut with the shutter door to prevent the rat from continuing

to central nose poke (Fig. 1). After a fixed 2.5 s inter-trial interval (ITI), the central port

was illuminated by an interior LED of the central port signaling the ready state of a trial

initiation. The rats initiated each trial by making nose pokes into the central port. After a

0.2–0.6 s random stimulus delay, the visual stimulus was presented from the left or right

side for a duration of 0.2 s. Rats were allowed to make a choice response after the end

of the stimulus delay period. The trials where animals prematurely left the port before

stimulus delay were canceled and they needed to re-initiate the trials. I randomly

provided one of three levels of visual brightness (difficult, normal, and easy) for each

trial by modulating the voltage ranging 0.02–5.1 lx. Medium stimuli were chosen for

each subject such that the subject detected stimuli with medium accuracy between easy

and difficult stimuli in forced-choice trials. The probabilities for left, right, or no visual

stimulus were equal (33% per condition) in 3C and FC trials (Fig. 1). The reward was

given if rats chose the same side where the visual stimuli was emitted in the 3C and FC

trials. If animals kept nose poke more than X s in the central port after the presentation

of the visual stimuli, the trial was treated as miss error. X were drawn from the uniform

distribution with a range of [0.5, 1]. Note that X is aligned with the expected timing of

the reward delivery in no-signal trials so that animals cannot utilize the absence of

reward delivery as indication of the presence of unnoticed visual stimuli. Failure of the

peripheral choices within 5 s after nose withdrawal from the central port was also

treated as miss error, though it occurred rarely (<5%). There was no punishment in any

error trials and next trial was allowed to be initiated after ITI. In the no-signal trials,

animals need to wait for 0.2–0.6 s without stimulus and another 0.5–1 s to get reward

from the central port. There was no cue to distinguish the initial delay (0.2–0.6 s) and

reward delay (0.5–1 s). Thus, animals did not have any external clue to differentiate the

signal trials from the no-signal trials, except for the presentation of the signal itself. In

the FC trials, the shutter was closed 0.5 s after stimulus presentation onset, and the rats

were forced to choose either the left or right port (Fig. 1). In cases where no stimuli

were presented in FC trials, the animals were never rewarded (Fig. 1B). After task

training (see methods in chapter 2 in details) was complete, to confirm whether rats had

a steady choice criterion, I alternated probe sessions with graded stimulus strength (session A) and neuronal recording sessions with a constant near threshold stimulus strength (session B). Session B followed the same protocol as session A, except that only a single stimulus difficulty was used. I applied a medium stimulus contrast level in FC trials in session A.

Electrophysiological recordings

A custom-designed electrode composed of two eight-tetrodes (tungsten wire, 12.5 μm, California Fine Wire, Grover Beach, CA) was used for the simultaneous recordings of V1 and PPC. The tetrodes were individually covered by a polyimide tube (A-M Systems, Sequim, WA), placed at a 100 μm separation, and typically had an impedance of 120–1000 kΩ at 1 kHz. The signals were recorded with Open Ephys (Cambridge, MA) at a sampling rate of 30 kHz and bandpass filtered between 0.3 and 6 kHz. The tetrodes were lowered approximately 40 μm after each recording session.

Spike sorting and screening criteria of units

All analyses were performed using MATLAB (MathWorks, Natick, MA, USA). To detect single-neuron responses, the spikes were manually clustered with MClust (A.D.

Redish, University of Minnesota) for MATLAB. Only neurons that met the following

criteria were included for further analyses: (1) units with sufficient isolation quality

(isolation distance $\geq$ 15, isolation distance is a measure of unit isolation quality in high

dimensional feature space from tetrode recording);(Harris et al., 2001) (2) units with

reliable refractory periods (violations < 1% of all spikes); and (3) units with sufficient

mean firing rates in the $-0.3 - 0.5$ s after cue onset (> 1 Hz).

Behavioral data analysis

Spatial choice accuracy was defined as the percentage of correct port choices in

trials where either outer port was chosen upon presentation of a peripheral stimulus

(Figures 13A). The miss rate was the percentage of central port choices in trials where

visual stimuli were presented in 3C trials (Figures 13B). The correct rejection rate was

the percentage of central choices in trials where visual stimuli were omitted in 3C trials

(Figures 13C). Reaction time was defined as the duration from stimulus presentation

onset to nose withdrawal from the central hole. Trials with reaction times < 100 ms

were considered invalid and excluded from the calculation of spatial choice accuracy as

they were considered too soon to respond to the stimulus. All error bars are presented as

mean $\pm$ SEM. All violin plots combine a boxplot with a kernel density estimation

procedure. The boxplot inside the violin shows the quartile, whisker, and median values

as white dots (Figures 13G-H).

I classified the following three choice types based on the subjects' detection

performance (Figures 1A–B): (1) Hit were trials when subjects successfully chose a left

or right port in 3C or before shutter closure in FC. (2) Miss-correct (Miss+) were trials

when the nose remained in the central port over 0.5 s and subjects chose the correct port

after shutter closure. (3) Miss-incorrect (Miss-) were trials when the nose remained in

the central port over 0.5 s and subjects chose the incorrect port after shutter closure.

Trials with missing responses in 3C were excluded from the analysis of comparison

across choice types because they could not be categorized into Miss+ or Miss-. I set a

maximum time for peripheral choice of 0.5 s~after the shutter closed in FC trials.

However, in this dataset there was no single instance where rats did not choose the

peripheral port after the shutter closed.

To estimate the impact of task parameters on behavioral performance, I conducted a

generalized linear model (GLM) analysis for spatial choice (left/right) and hit/miss

choice (Figures 13E and 13F). In the models, I used the logit function as link function.

For spatial choice GLM analysis, I prepared trials in which they performed peripheral

choices. Task parameters included binary stimulus predictors (1 was stimulus presence,

and 0 otherwise), previous peripheral reward (1 was rewarded, 0 otherwise), and

previous central reward (1 was rewarded, 0 otherwise). The model was fit with these

predictors. For hit/miss choice GLM analysis, I first prepared trials in which stimulus

was present. Task parameters included binary predictors of previous peripheral reward

(1 was rewarded, 0 otherwise), previous central reward (1 was rewarded, 0 otherwise),

and previous failure (1 failed, 0 otherwise). Then, I fitted the model to behavioral

performance using the same procedure as the spatial choice GLM analysis. To quantify

the impact of each task parameter, I calculated the difference between explained

variance (R^2) of the full model and partial model. The partial model lacks a target task

parameter.

Time-locked kernel regression and visual sensitivity

Identifying the task and behavioral variables of responsive neurons by comparing

trial-by-trial firing patterns is challenging because some variables are presented or occur

in a close time. For example, stimulus presentation and movement onset are sometimes

intermingled with time (Figure 8). Suppose the neuron significantly responded to the

intermingled time. In that case, it is difficult to identify the sensitivity of the neuron to

the stimulus, movement, or both using the mean firing rate of the interested epoch, such

as the receiver operating characteristic (ROC) method. To overcome this difficulty,

recent studies introduced a regression model for characterizing statistical dependency of

firing rate to the task and behavioral variables (Pillow et al., 2008; Park et al., 2014; Aoi

et al., 2020; Keeley et al., 2020). The basic idea is to fit the model that predicts neuronal

activity using the task and behavioral variables. This considers the time-dependent

firing rate with respect to the occurrence of the task and behavioral variables taking

advantage of trial-by-trial variability of the timing of task and behavioral variables.

To identify the task and behavioral variables of responsive neurons, I used a time-

locked kernel regression approach (Figures 9A-B) (Steinmetz et al., 2019). In this

approach, the firing rate of recorded neurons is described as a linear sum of task

predictors aligned to task events. In this study, I considered the stimulus onset and

reaction timing as task events. According to this kernel, the predicted firing rate $f_n(t)$

for a neuron n is described as

$$f_n(t) = \sum_l \sum_{t_s \in S} K_{l,n}(t - t_s) + \sum_{t_M \in M} K_{M,n}(t - t_M) + \sum_{t_D \in D} K_{D,n}(t - t_D)$$
$$+ \sum_r \sum_{t_R \in R} K_{r,n}(t - t_R) + \sum_{t_F \in F} K_{F,n}(t - t_F) + \sum_w K_{w,n}(t) + \varepsilon$$

where l represents the stimulus direction (ipsi or contra), r represents the previous

reward direction (ipsi, contra, or center), w represents the whole-trial kernel types

(reaction time; RT or moving time; MT) and S, M, D, R, F represents the set of times to cover each predictor window. $K_{l,n}, K_{M,n}, K_{D,n}, K_{r,n}, K_{F,n}, K_{w,n}$ represents the stimulus, motor-preparation, choice preparation, previous reward, previous failure, and whole-trial (RT or MT) kernels for neuron n. The stimulus kernels cover the window 0–0.3 s from stimulus onset, the motor preparation and choice preparation kernels cover the window -0.3–0 s from the reaction timing (central withdrawn timing), previous reward and previous failure kernels cover the window -0.1 – 0.1 s from stimulus onset. The motor preparation and the choice preparation kernels are identical except that the latter is designed to be sensitive to choice directions (ipsi-direction is a negative value). The stimulus, motor preparation, previous reward, and previous failure kernels coded as "1" or "0", and the choice preparation kernel has a value of "-1," "0," and "1," which negative and positive value indicated that ipsi- and contra-direction, zero indicated central-choice. The whole-trial kernels consist of the reaction time (RT) and moving time (MT), which has one value that remained constant for the entire trial. The values for RT and MT were min-max normalized to 0-1 range. To fit the firing rate to the model, the firing rate was binned into 0.01-s bins and then smoothed with a causal Gaussian filter with a standard deviation of 0.03 s. The stimulus (ipsi and contra) and preparation (motor and choice) kernels then contain $L_S, L_M, L_D = 30$ time bins, the

previous reward (ipsi and contra) and failure kernels contain $L_R, L_F = 20$ time bins,

and the whole-trial kernels (RT and MT) contain $L_W = 1$ time bins. I therefore made

the design matrix DM by concatenating parameterized kernel matrices for a subset of

trials of size $L \times T$ ($L = 2 \times L_S + L_M + L_D + 2 \times L_R + L_F + 2 \times L_W = 162$ time

bins, and $T = 50 \times N_{trials}$ time bins) (Figure 9A).

To estimate the optimal weights for each neuron's kernels without overfitting, I

estimated a weight vector w_n to solve the penalized residual sum of squares with

elastic net regularization consisting of 99% L2 and 1% L1 methods during the time-

locked kernel regression (Banerjee et al., 2020) (using MATLAB package cvglmnet

https://web.stanford.edu/~hastie/glmnet_matlab/intro.html). During weight estimation, I

used the parameters in elastic net regularization λ which is calculated by minimizing

cross-validated (3-fold) error within training dataset. The predicted firing rates were

constructed as $P_n = DM^T w_n$.

To determine whether each neuron is sensitive to each task and behavioral kernels, I

prepared a predictor matrix with full kernels (real design matrix) and a matrix in which

the target kernel is set to zero within whole-time points (Partial model, Figure 9A right).

I then fit the model with each design matrix to predict firing rates and calculated the

explained variance (R^2_{full}, $R^2_{partial}$) of the full and partial models, in either case with

tenfold cross-validation by leaving out a random 10% subset of trials to calculate the

model performance. Each fold consisted of equal proportions of contra-stimulus, ipsi-

stimulus, and no stimulus emitted trials (Figure 9A bottom). The explained variance was

calculated from model-predicted and actual neuronal activity in test trials. I used an

elastic-net regularization consisting of 99% L2 and 1% L1 methods during the tame-

locked kernel regression to prevent over-fitting(Banerjee et al., 2020). If the explained

variance of the partial model ($R^2_{partial}$) was significantly reduced compared to the full

model (R^2_{full}), the neuron was deemed selective for the target kernel (Figure 9B, paired

t-test, Holm-Bonferroni correction for all comparison). Neurons selective to the

stimulus contra kernel were labeled stimulus-preferring neurons, and the other neurons

were labeled stimulus non-preferring neurons. Note that neurons selective to the

stimulus ipsi kernel were excluded from the analyses in Figure 14-25. Nevertheless,

those neurons were relatively few and their inclusion/exclusion did not affect my

conclusion.

Spike train analysis

I recorded 951 neurons (V1: 515, PPC: 436 neurons) from 62 sessions in seven rats.

Unless otherwise stated, the activity of each neuron was binned at 0.01 s and smoothed

with a causal Gaussian filter with a standard deviation of 0.03 s to obtain the temporal

profile of each neuronal activity.

For visualization (Figures 14C) and analysis, firing rates were z-scored relative to

trial-by-trial baseline rates (from the window −0.5 to 0 s).

Statistics

I evaluated the statistical significance in the analysis using data resampling with a

bootstrapping procedure.(Parthasarathy et al., 2017) I estimated the p value for the

bootstrapping procedure by computing the ratio (1+X) / (N+1), where X indicates

overlapping data points between the two distributions, and N indicates iterations. Since

I used 1,000 bootstraps, two distributions with no overlap resulted in p < 0.001, and two

distributions with x% overlap resulted in P »x/100 (Figure 10).

State-space analysis

For state-space analysis, I used neurons with ≥ 20 available trials for each Hit+ and

Miss+ condition. To characterize the population structure and the temporal pattern

among all neurons during the analysis window (-0.1 – 0.15 s from stimulus onset), z-

scored firing rates were formatted as $X \in \mathbb{R}^{N \times CT}$, where N is the total number of

neurons, C is the total number of conditions (choice types), and T is the number of

analyzed time points. Principal component analysis (PCA) was used to reduce the

dimensionality of the population from the number of neurons to ten principal

components (PCs). Each PC represents a weighted combination of individual neuronal

activity, which summarizes population activity.

To estimate the difference of each neural trajectory at each time point across choice

types in the PC space, I prepared a dataset by bootstrapping 1,000 times with different

subsets of twelve trials for each choice type. For the control dataset, trials were shuffled

within Hit+ and Miss+ conditions. I then calculated the sensitivity index (d') for each

PC as follows:

$$d'^2_i(t) = \frac{\left(\mu_i^{Hit+}(t) - \mu_i^{Miss+}(t)\right)^2}{\frac{1}{2}\left(\left(\sigma_i^{Hit+}(t)\right)^2 + \left(\sigma_i^{Miss+}(t)\right)^2\right)}, i \in [3\,(10)], t \in [-0.5s\ 1.0s]$$

where $\mu_i^{Hit+}(t)$ and $\mu_i^{Miss+}(t)$ are the mean values of the i-th PC at time t in Hit+

and Miss+ trials, respectively, and $\sigma_i^{Hit+}(t)$ and $\sigma_i^{Miss+}(t)$ are the standard deviation

of the i-th PC at time t in Hit and Miss+ trials, respectively. I used the sensitivity in

the first three or ten PCs subspace defined as the square root of $d'^2(t)$ (Figure 18B),

as follows:

$$d'^2(t) = \sum_{3\,(10)} d'^2_i(t)$$

For statistical significance of the trajectories between Hit+ and Miss+ (Figure 18A),

I calculated P-value as described in statistics section with the level of significance at

0.05.

State space analysis at each task and behavioral axis

For the state-space analysis at a specific task and behavioral axis (Figures 11 and

20), I applied a variant of the "Coding Direction" analysis (Li et al., 2016; Allen et al.,

2019). I first calculated the condition-averaged z-scored firing rate (Hit+/Miss+, or

stimulus presence/absence) for each neuron for relevant epoch. To obtain the coding

direction, I computed the difference of firing rates between conditions (Figure 11).

Specifically, I defined the following four axes. The "state axis" was computed from the

dissociation of neuronal activity between the Hit+ and Miss+ trials in the pre-stimulus

window (-0.5 – 0 s from stimulus onset). The "movement axis" was computed from the

dissociation of neuronal activity between the Hit+ and Miss+ trials in the movement

window (0.3 – 0.5 s from stimulus onset). The rats moved to the contra-lateral port in

the Hit+ trials because the Hit+ trials were defined as a peripheral choice before 0.5 s

from stimulus onset; rather, the Miss+ trials consisted of only delayed response after 0.5

s from stimulus onset. The "stimulus axis" was computed from the dissociation of

neuronal activity between stimulus presence and absence trials in the during-stimulus

window (0 - 0.15 s from stimulus onset). Finally, the "decision axis" was computed

from the dissociation of neuronal activity between the Hit+ and Miss+ trials in the same

window (0 - 0.15 s from stimulus onset). The decision axis captures variable

components such as decision formation, motor-preparation, and other subjective states. I

prepared the four vectors, which are mean population activity w_a of length $N_{unit} \times 1$,

indexed by the four axes. I then obtained the orthogonal axes by orthogonalizing the

four vectors w_a with the QR-decomposition:

$$W = QR$$

where $W = [w_{State} \ w_{Movement} \ w_{Stimulus} \ w_{Decision}]$ is a matrix whose columns

corresponding to the difference of firing rates of each axis. Q is an orthogonal matrix,

and R is an upper triangular matrix. I then obtained the orthogonalized axis vectors

$w_a^{\perp}$ by the first four columns of Q. These vectors span the orthogonal subspace in

neuronal population activity space.

The projections of each axis were computed by dot product as $w_a^{\perp}x$, where x is an

$N_{unit} \times (2 \times time)$ matrix of smoothed, trial-averaged firing rates across Hit+/Miss+

conditions.

For the statistical significance of the differences in choice-type projections for each

axis, I computed the W using a subset of trials (40%) in each condition and then

projected the data from the remaining subset of trials (60%) onto each axis. The

procedure was repeated 100 times with shuffling trials within each condition. The sign

of the projection in Hit+ was aligned to be positive in each analysis epoch. I then

compared the resampling distributions between Hit+ and Miss+ or distance and zero. If

the distributions are not overlapped in 2SD range (95.5% data in this range), they are

defined as significantly dissociated.

To confirm whether the statistical significance of the resampling method described

above is statistical noise, I conducted the simulation analysis using a noise dataset

(Figure 21). I generated the random digits ranged -1 to 1 for 20-40 trials in arbitrary

conditions 1 and 2 as the one noise dataset and prepared 266 simulated neurons, the

same number of actual data in V1. Then, the same analysis described above was

performed with 100 iterations.

Classification (decoding) analysis

For classifiers, I used support vector machines (SVM) with a linear kernel function

implemented using the MATLAB *fitcsvm* library. All population classification was

analyzed on the concatenated neuronal activity of individual neurons. Because the

number of simultaneously-recorded neurons was low in my dataset, I constructed

"pseudo-trials" by randomly extracting trials from desired conditions for each

neuron(Mante et al., 2013). For the training and testing dataset, the number of trials in

each condition was matched to prevent bias for training classifiers. I used tenfold cross-

validation by leaving a 10% subset of trials for prediction to avoid overfitting. This

procedure was repeated 100 times. Hyperparameter such as C regularization weight

was determined by optimization to minimize loss of validation dataset in a grid search

manner (searched range $10^{-5} - 10^{5}$)(Najafi et al., 2020).

For two-class classification, such as stimulus classification (presence/absence)

(Figure 14E) and choice type (Hit+/Miss+) (Figures 22A-22C, 23A, 23C, and 24A-

24B), I used the firing rate during stimulus window (0 – 0.15 s from stimulus onset) and

pre-stimulus window (-0.2 – 0 s from stimulus onset) for each individual neuron,

respectively. I then concatenated neuronal activity as described above and performed

training and predictions. For classification metrics, I used classification improvement

over shuffled (only in Hit+/Miss+ classification), which is calculated by classification

accuracy in real data minus shuffled data. This ensures that high values represent the

presence of neuronal information and minus low values its absence(Montijn et al.,

2014). To test statistical significance, if the zero was < 2SDs (95.5% distribution) of the

distribution of bootstrapped classification improvement, the data was deemed

significantly informative.

To classify the choice types with the simultaneously recorded population (Figures

20A and 20B), I first extracted sessions with ≥5 neurons in each region and ≥20 trials in

each condition (20 sessions). I trained the classifier using the same procedure described

above and predicted the test data. In the de-correlated population in V1 and PPC (Figure

24B), the trial order was shuffled within each choice type for each neuron. I then

calculated the classification accuracy of real data and the de-correlated population using

the procedure described above.

To measure the contributions of each neuron for the choice types (Figure 22D), I

compared weight distributions of the classifier for different neuronal types, that is,

contra-stimulus selective neurons and the other selective neurons. The neuronal weight

was normalized to unity length. For statistical significance, I performed a one-way

ANOVA test with LSD post hoc comparisons.

Stability (cross-temporal classification analysis)

To estimate the stability of population coding, I applied a cross-temporal classification analysis where the classifiers were trained and tested with unique time samples (Figure 23). Each classifier trained at time $t_{trained}$ can also be tested on its classification ability to predict the choice outcome at time t_{tested}. For visualization, I computed the classification improvement over shuffled data as described above (see classification analysis). The negative value was rounded to zero, and the above 0.5 value was rounded to 0.5. When I test the statistical significance of predictability, I used the same metrics with the classification improvement described above using unrounded value.

To estimate the stability of population coding, I calculated Pearson's correlation coefficients between the neuronal weights of each classifier at time $t_{trained}$ and t_{tested} (Figures 23A). To quantify the time-resolved decay of population activity pattern, I used Pearson's correlation coefficients $0 - 0.5$ s from time $t_{trained}$ (Figure 23C) in -0.2 s–0 s training time. For comparison between populations, I used Kolmogorov–Smirnov test followed by post-hoc Tukey tests for subpopulations and regions (Figure 23D).

Noise correlation

Noise is defined as the trial-to-trial variability of the neural response from the mean under a given choice type condition. Noise correlation was defined as the correlation coefficient between the noise of a given neuron pair within the same choice type conditions. I arranged the firing rates of single neurons in a trial-by-time matrix per choice type with a time resolution of 50ms spanning -0.4 – +0.4 s after the stimulus onset. The matrix was z-scored with the mean and the standard deviation of the trials at each time point for each choice type. Then, I calculated Pearson's correlation coefficients of the z-scored firing rates (i.e., noise) for each pair of neurons at each time point (Figures 24C, 24D and 25).

Cell-type classification

To classify the putative fast-spiking (FS) interneuron and regular-spiking (RS) excitatory neurons, I calculated trough to late peak and firing rate for each recorded unit (Figures 12A and 12B). I then determined the cell types by clustering the units in the dimension of the parameters using the k-means algorithm (k = 2) with these two variables using the MATLAB *kmeans* function. After clustering units, I defined clusters that had a lower trough to late peak compared to the other cluster as putative FS interneurons and the other as RS excitatory neurons (Figure 12).

3.4 Results

Rats performed visual detection task based on their internal threshold

I trained seven rats to perform a spatial visual-cue detection task (Figures 1A–1B), which is essentially a three-alternative choice design that encourages animals to report the presence or absence of peripheral visual stimuli as described in my previous study. Briefly, the rats initiated a trial by poking their nose at the central port. They were rewarded by choosing outer ports (left or right) when a visual stimulus was presented or by keeping the nose in the central port when no peripheral stimulus was presented. In half of the trials, the central port was closed 0.5 s after stimulus presentation to force animals to choose one of the outer ports. To confirm whether rats had a steady choice criterion, I alternated probe sessions with graded stimulus strength (session A) and neuronal recording sessions with a constant near-threshold stimulus strength (session B). In session A, the peripheral choice accuracy in forced-choice (FC) trials decreased from approximately 80% to 65% as visual contrast decreased (Figures 13A, orange), and the accuracy was maintained at >90% regardless of visual contrast in the three-choice (3C) trials (Figures 13A, blue). Note that trials where rats chose to stay in the central port were excluded from calculating spatial choice accuracy in 3C trials. Rats missed the visual

stimuli more often (from 50% to 70%) as visual contrast decreased (Figures 13B). They

also showed >90% correct rejection performance when the visual stimulus was omitted

in 3C trials (Figures 13C). In 3C trials, the reaction times for correct choices have a sharp

peak at around 0.2 s (Figures 13E and 13F), showing that highly stereotypic responses to

visual stimuli are repeated when the rats make correct choices. The reaction time

distribution was slightly shifted to earlier time points in easier trials. By contrast, reaction

times in erroneous trials were scattered without a specific peak, suggesting that incorrect

choices were made at random without a specific clue. These results confirmed that rats

have a generalized strategy to choose the outer ports in response to peripheral stimuli only

when their choice criterion is met. In addition, rats showed correct choices above the

chance level when the shutter forced them to select one of the outer ports after first

choosing to stay in the central port (Figures 13D, gray). Thus, the rats received visual

information but did not always maximally exploit it. I labeled trials with different choice

types as hit correct (Hit+), hit incorrect (Hit−), miss correct (Miss+), and miss incorrect

(Miss−) according to choice performance (Figures 1A and 1B).

To determine what drove the rat's choice, I applied a generalized linear model (GLM)

analysis to the behavioral data. I used multiple variables, such as current stimulus,

previous reward positions, and previous failure (unrewarded), as independent variables

and predicted spatial choice direction and go or no-go responses to left and right stimuli (Figures 13E and 13F, respectively). I compared regression coefficients and uniquely explained variance by the variable (see Methods). Note that individual ΔR^2 does not add to the total R^2 because some of the variance can be explained by multiple factors. In the Hit trials, the majority of the spatial choice variance (67%) was accounted by the stimulus direction alone with minimal contributions (2%) from previous reward positions (Figure 13E). In contrast, although the total explained variance was much lower (~30%) in the Miss trials, previous reward positions had a stronger effect on spatial choice (6%; Figure 13E). I also confirmed mild contributions (about 10%) of previous reward positions in go or no-go decisions (Figure 13F). Together, spatial choices in the hit trials were predominantly driven by visual information with little influence of previous reward positions, although spatial choices in the miss trials were partially influenced by the incongruent previous reward positions to the stimuli.

Stimulus-preferring neurons in V1 and PPC were activated regardless of choice types

I recorded neurons simultaneously from the right V1 (NV1 = 515 neurons) and right PPC (NPPC = 436 neurons) using chronic tetrode implants during task performance

(Figure 7). To investigate how visual neuronal responses contribute to behavioral responses, I first identified stimulus-preferring neurons using time-locked kernel regression analysis with multiple task predictors, such as contra- and ipsi-lateral stimuli, motor preparation, and choice-preparation kernels (Figures 9 and 14; see Methods). Approximately 30%–40% of the neurons were defined as selective to visual stimulus in V1 (40%; N = 203) and PPC (27%; N = 116; Figures 14B and 15A). Based on the results, I classified the neurons as enhanced-type stimulus-preferring neurons and suppressed-type stimulus-preferring neurons and the remainder as stimulus non-preferring neurons (Figure 14B-C). These subpopulations consisted of heterogeneous neurons with different selectivity (Figure 14D) and different spatial distribution (Figure 15C). Importantly, both V1 and PPC neurons showed stimulus-dependent activity (enhanced and suppressed from pre-stimulus baseline), regardless of choice types (Figures 14C and 15B). Furthermore, the stimulus non-preferring neurons in both V1 and PPC did not show apparent differences in the average temporal dynamics among choice types until 0.2 s after stimulus presentation, where behavioral responses occurred (Figure 14C).

To further clarify whether the presence of visual information in V1 and PPC is important for hit and miss behaviors, I conducted a population-decoding analysis of the stimulus

(presence or absence). I found that the stimulus-preferring population decoded stimulus presence near perfectly in the Hit+ and Miss+ trials (Figure 14E), demonstrating the robust presence of visual information both in the Miss+ and Hit+ trials. This also indicated that the stimulus period's activity was evoked by a visual stimulus, but not by stimulus expectations. I also confirmed that the stimulus non-preferring population could not predict the stimulus presence or absence even as an ensembled activity (Figures 14E and 15D). Furthermore, the classification accuracy for the Miss− trials was relatively high (~ 80%) in V1 but was at chance level in PPC, indicating that the visual information in PPC was not as robust as V1 in the Miss− trials. These results indicate that, in contrast to the Miss− trials, the lack of go responses in the Miss+ trials is not explained by the robustness of visual information in the visual cortex.

Significant contributions of non-sensory neurons in V1 and PPC for separating different choice types as population activity

So far, I found no significant differences in neural activities in the Hit+ and Miss+ trials. However, the metric of mean activity is sometimes not the best way for seeking the neural population codes between conditions. For example, if we recorded three neurons

at the different conditions, even if the mean activity is similar between conditions (Figure 16 right), the neural population geometry, which can be drawn in the high dimensional neural space, is sometimes embedded significantly different paths (Figure 16 left). Taking care of this neural dissociation between conditions in high dimensional space (refereed to population state) is important to address the population encoding of condition. Then, I wanted to address whether neuronal population states differentiate choice types (hereafter only referred to as Hit+ and Miss+ trials). To this end, principal component analysis (PCA) was applied to a population data consisting of trial-averaged choice-type neuronal activities ranging from −0.1 to 0.15 s after stimulus onset (see Methods for details). The PCA finds the axes optimized to capture the variance of neuronal activity across choice types and time. I identified three dimensions that captured 73% of the total variance for the whole population in both V1 and PPC (Figure 17A). The reconstructed population activities from those three PCs have distinct dynamics between the Hit+ and Miss+ trials in V1 and PPC (3D plots in Figure 17B and individual PCs in Figures 18A). I found a significant separation between choice types in the analysis window in both V1 and PPC (Figures 17B and 18), suggesting that separation of the Hit+ and Miss+ responses is the result of the coordinated activity of many neurons. The difference of neuronal activities between the Hit+ and Miss+ trials up to 0.15 s after stimulus onset is not likely to be

related to behavioral differences between Hit+ and Miss+ conditions because trials with reaction time <0.2 s were not included in the analysis (see Methods). On the other hand, the activity difference between Hit+ and Miss+ trials before 0.15 s after stimulus onset should reflect the difference in internal states for driving spontaneous choices in response to visual stimuli, given that rats can elicit correct spatial choices in both choice types.

Interestingly, V1 and PPC population activities shared similar PCs that may reflect neural activities to different task events and background fluctuations. For instance, PC1 shows distinct dynamics peaking around 100 ms after the onset of visual stimuli (Figures 18A). In both V1 and PPC, PC1 discriminated Hit+ and Miss+, although the time course of this effect's significance varied slightly between the two brain regions. PC2 sustained the separation of choice type information robustly before stimulus onset (Figures 18A). PC3 and others (Figure 18A) show oscillatory-like components with different frequencies, in which the phase separates choice types, suggesting a relative timing of global fluctuations across V1 and PPC to stimulus onset provides a significant influence on choice types. However, none of these components are dominated by neurons with particular selectivity (Figure 19), except for the PC1 for PPC, dominated by stimulus-preferring neurons. In both V1 and PPC, I further confirmed a robust separative population-level activity between choice types in the stimulus non-preferring population

in V1 and PPC (Figures 18A, and 18B). Other than the presence of visual-response-like components in stimulus-preferring populations, major PCs were qualitatively similar between stimulus-preferring and stimulus non-preferring populations. These results indicate that Hit+ and Miss+ responses are mediated by multiple processing levels from a variety of neurons, including stimulus non-preferring neurons.

Decomposing population dynamics showed distinct state dynamics across choice types

The results above suggest the importance of non-sensory activities for separating choice types, but the association between the different task events and the population-level components is not clear. In particular, though I identified PC1 as a visual-response-like component in both V1 and PPC, it is still unclear whether other components are orthogonal to the visual-stimulus-evoked activity because the PC1 is a mixture of various neurons, including stimulus non-preferring neurons (Figure 18), and may contain the non-stimulus factors (e.g., brain state). To further distinguish the source of non-sensory activities, I generated a neural state space spanned by orthogonalized axes that capture the population activities related to stimulus presence, internal states, decisions, and movement (Figures 11 and 20A; see Methods). I defined a "stimulus axis" by computing the maximally separated activity between stimulus-present and stimulus-absent trials

during stimulus window (0–0.15 s from stimulus onset), a "state axis" of activity by computing the maximally separated activities between the Hit+ and Miss+ trials during the pre-stimulus window (−0.5 to 0 s from stimulus onset), a "decision axis" of activity by computing the maximally separated activities between the Hit+ and Miss+ trials during the stimulus window (0–0.15 s from stimulus onset), and a "movement axis" by computing the maximally separated activity between the Hit+ and Miss+ trials during movement window (0.3–0.5 s from stimulus onset; Figures 11). Though the selection of the analysis windows is arbitrary, I wanted to address whether and how distinct population dynamics associated with different events can separate choice types beyond the analysis window. I projected the population activities from the Hit+ and Miss+ trials onto each axis, which captured 25%/21%, 66%/51%, 16%/15%, and 26%/30% explained variance in the state, movement, stimulus, and decision axes in V1 and PPC, respectively (Figure 20B). I validated the separations of projections between the Hit+ and Miss+ trials using independent trials from train sets (see Methods; $p < 0.05$; Figure 20C). I found that the population activities projected onto the pre-stimulus state axis segregated choice types as sustained dynamics beyond stimulus onset in both V1 and PPC, whereas those projected onto the decision axis showed only minor differences. On the other hand, the population activities projected onto the movement axis were largely contained within movement

epoch (0.3 s after stimulus onset) without affecting stimulus epoch. Finally, I found that, consistent with decoding analysis, the stimulus-evoked population activities did not segregate choice types, at least before movement onset (<0.2 s; Figure 20C). As expected, control analysis with randomly generated data did not show such robust and unique population dynamics (Figure 21). These results suggest distinct population dynamics orthogonally embedded to stimulus-evoked activities for separating choice types in both V1 and PPC.

The population representation of choice types is distributed across heterogeneous individual neurons

The analysis so far revealed that choice types can be discriminated with trial-averaged neuronal dynamics, but I wanted to examine whether that was the case on a single-trial basis. To this end, I applied a linear support vector machine (SVM) algorithm to predict the choice types (Hit+ and Miss+) of trials at each time point in V1 and PPC populations (Figure 22A). Compared with trial-label-shuffled control, I found significant improvements in the Hit+ and Miss+ classification at the time points during pre-stimulus, stimulus, and post-stimulus epochs. Note that the classification improvement in post-

stimulus epoch (0.2–0.5 s from stimulus onset) simply reflects differences in behavior between the Hit+ and Miss+ trials. Next, I performed the same analysis dividing the population into stimulus-preferring and non-preferring neuronal subpopulations in V1 and PPC (Figure 22B). Improved classification in the pre-stimulus period was observed in the non-preferring population in both V1 and PPC and stimulus-preferring neurons in PPC (Figures 22B and 22C). The non-preferring population showed a significant classification improvement in both epochs in V1 and PPC (Figure 22C), whereas the stimulus-preferring population did not show a robust improved classification during stimulus epoch in the PPC. These results confirmed the robust contributions of the non-preferring population for separating choice types even on a trial basis throughout different time points prior to movement. Analysis of single neuronal contributions to the population decoder suggests widely distributed contributions of different neuron types in separating choice types during both pre-stimulus and stimulus epochs (Figure 22D). However, I also found biased contributions of neuron types depending on task epochs and areas: in the pre-stimulus epoch, the previous contralateral-reward-preferring neurons significantly contributed to choice-type coding compared to the stimulus-preferring neurons in PPC (Figure 22D; $p < 0.05$; one-way ANOVA followed by least significant difference LSD multiple comparisons), although, during-stimulus epoch, stimulus-preferring neurons

contributed to the coding compared with the previous ipsi-reward-preferring neurons in V1 (Figure 22D; $p < 0.05$; one-way ANOVA followed by LSD multiple comparisons).

I next asked whether the population computation for choice types dynamically changed or was stable over time. A cross-temporal classification analysis was performed to probe the stability of neuronal population computation (Figures 23A and 23B). As expected, the highest stability of classifiers was found around the time where the behavioral differences between Hit+ and Miss+ trials occurred (0.2–0.5 s after stimulus onset). Other than that, pre-stimulus classifiers were relatively stable at least until 0.1 s from stimulus onset in all neurons and stimulus non-preferring neurons in PPC, whereas the stimulus-preferring population showed less stability in the cross-temporal classification (Figure 23B). To estimate the stability of neuron contributions for the classification of choice types across time, I calculated Pearson's correlation coefficients of neuronal weights of pairs of classifiers at different times (Figures 23C and 23D). If the population computation is similar across time, the correlation coefficients will be tolerant to decaying. For a comparison between whole populations in V1 and PPC (Figure 23D, top; $p < 0.01$; Kruskal-Wallis test), V1 was relatively dynamic compared to PPC. Such a dynamic population computation was, in particular, evident in both stimulus-preferring and non-

preferring neurons in V1 (Figure 23D, below), whereas the stability was relatively higher

in non-preferring populations in the PPC than elsewhere (Figure 23D, below; $p < 0.05$;

the Kruskal-Wallis test followed by post hoc Tukey's tests for comparison). Together,

these results suggest that choice information was stable over time, especially in stimulus

non-preferring neurons, although population computation is dynamic, especially in V1.

V1 noise correlation increased in forced detection performance before and after stimulus
presentation

Thus far, my results demonstrate that non-preferring neurons encode choice types in

V1 and PPC. However, in these analyses, I used a "pseudo-population" that combined

neuronal activity recorded in different trials. Therefore, my analysis did not consider the

correlation structure of pairs of simultaneously recorded neurons within each trial (i.e.,

noise correlation). If the noise is closer to random across neurons (low noise correlation),

information coding can be more reliable and efficient (Rumyantsev et al., 2020) (but see

(Moreno-Bote et al., 2014)). I first examined classification accuracy in each session using

a simultaneously recorded population. Both V1 and PPC populations showed a

significantly higher classification than shuffled data (Figure 24A; $p < 0.001$ in V1 and

PPC). Next, I compared classification accuracy with a de-correlated population where each neuron in the same session was randomly selected from different trials within the same choice type (STAR Methods). Thus, the de-correlated population maintains the signal correlation while removing the noise correlation. Both V1 and PPC populations had significantly decreased classification accuracy in the de-correlated population (Figure 24B), indicating that the correlation structure was crucial for population computation.

To investigate the correlation structure in choice types, I calculated pairwise noise correlations separately for Hit+ and Miss+ conditions at each time bin (see Methods; Figure 24C). I found that noise correlation in Miss+ trials increased in pre-stimulus epoch and during stimulus epoch compared to Hit+ trials in V1 neuron pairs, although PPC neuron pairs did not differ in choice types (Figure 24C). Such a difference in noise correlation was mostly apparent in neuron pairs among regular-spiking neurons (Figure 25). I next asked whether reduced noise correlation is associated with pairs of neuronal types (i.e., stimulus-preferring and non-preferring neurons). The increased noise correlation in Miss+ trials was most evident in pairwise interactions between stimulus preferring and non-preferring neurons and non-preferring and non-preferring neurons, especially during pre-stimulus epoch (Figure 24D). These results suggest that neuronal coupling associated with stimulus non-preferring neurons in V1 plays an important role

70

in separating choice types.

3.5 Discussion

It is widely believed that the fidelity of visual responses in sensory neurons explains the trial-by-trial variance of visual detection performance. My results demonstrated significant contributions of non-sensory neurons in V1 and PPC to reliable visual detection performance. The near-threshold stimuli used in my task induced trial-by-trial variability in visual detection performance, and I further classified those trials with identical stimuli into three choice types, which were not differentiated in previous studies. Surprisingly, the Hit+ and Miss+ trials showed no differences in population encoding of stimulus as well as mean temporal dynamics (Figures 14C and 15B, right). Instead, I found multiple lines of evidence for population-level computation contributing to the

optimal behavioral responses to visual stimuli (Hit+ and Miss+) in V1 and PPC. First, I found a specific divergence between choice types at multiple levels of population activity, particularly with the robust contribution from stimulus non-preferring neurons in both V1 and PPC, which is orthogonally embedded to stimulus response dynamics (Figures 18, 20). Second, during pre-stimulus and stimulus epochs, the choice types were decoded on a single-trial basis with contributions of a variety of neurons with different selectivity in both V1 and PPC (Figure 22). Third, V1 neuron pairs, but not PPC, showed increased noise correlation in the Miss+ trials compared to the Hit+ trials before and during visual stimulus presentation, which was most evident in pairwise interactions between non-preferring neurons and others (Figures 24C and 24D).

It has been postulated that stochastic behavioral responses to identical sensory stimuli are generated by fluctuations of background neuronal ensembles preceding external inputs(Speed et al., 2019). A recent study further demonstrated that a global slow oscillation correlates with the level of task engagement measured by miss rates (Jacobs et al., 2020). My unsupervised analysis revealed at least three major distinct population dynamics in V1 and PPC, respectively (Figures 17B and 18). First, I found temporal dynamics coinciding with the visual response peak in both V1 and PPC. Second, I found sustained dynamics, which significantly contributed to separating the choice types well

before stimulus onset (Figures 18). The choice type was orthogonally represented to the visual response dynamics with involvement of non-sensory neurons (Figure 20). Third, I found that oscillatory components, which were prominent in both stimulus-preferring and non-preferring neurons of both V1 and PPC, were significant factors to differentiate choice types (Figures 18). Accordingly, I have two non-exclusive hypotheses on how stimulus non-preferring neurons can influence this process.

First, the extent of local interactions between stimulus non-preferring neurons and stimulus-preferring neurons may determine the deviation of choice between optimal (hit) and conservative (miss). Although my state space analyses (Figures 17 and 18) suggest that visual responses within stimulus-preferring population are orthogonally represented with the state signals, the mixed population of stimulus-preferring and non-preferring neurons in V1 represented visual responses with coherent modulation by state signals (PC1; Figure 18), suggesting significant interactions between stimulus-preferring and non-preferring neurons on a trial-by-trial basis that affect hit or miss behavior. Supporting this hypothesis, I found that the correlation structure among simultaneously recorded neurons around the stimulus presentation time can contribute to the separation of choice types (Figure 24B). Furthermore, I found an increased noise correlation in the Miss+ trials between stimulus non-preferring and others (Figures 24C and 24D), suggesting that the

relative timing of the visual stimulus with respect to the ongoing interactions among these neurons affects visual processing, resulting in biased decisions (i.e., Miss+ trials). Thus, I suggest proper interaction between stimulus-preferring and non-preferring neurons on a trial-by-trial basis underlies the optimal exploitation of visual information for behavior. However, I note that increased noise correlation is not necessarily harmful for information coding(Moreno-Bote et al., 2014; Montijn et al., 2016). Future studies will address whether and how downstream cortical areas exploit the integrated information for behavior.

Second, global oscillatory activities, including stimulus non-preferring neurons, support visual information transmission to downstream cortical areas. I observed various subtle oscillatory components, where the phase separated the choice types relative to the stimulus onset, suggesting that visual inputs can be efficiently exploited for behavior when the ongoing fluctuation is in a particular phase. The finding is consistent with previous studies that proposed that sensory information is gated by ongoing neural activities(Zylberberg, 2018; Allen et al., 2019; Shin and Moore, 2019; Speed et al., 2019). However, I did not obtain direct evidence that local field potential (LFP) corresponds to those spike oscillations. It is possible that LFP oscillation and spike oscillation from a particular subpopulation can be controlled differently. For instance, a recent study

suggested that non-sensory-tuned fast-spiking neurons originate cortical rhythmicity, resulting in the direct influence on sensory information coding in the primary somatosensory cortex(Shin and Moore, 2019). Future work will address the possibility that supports the local network mechanism and directionality of information flow between stimulus-preferring and non-preferring neuronal coupling.

The relatively weak contribution of visually evoked activities in V1 and PPC population coding could be a unique feature of my task design because animals had a third option, of which experienced reward value may suppress peripheral choices, even when the animals recognize the stimuli. It should be noted that ignoring the presence of stimuli is never rewarded in my task and, thus, is clearly suboptimal bias behavior. In addition, my data show that rewards in the previous trials only partially (about 10%) explain the behavioral variance in hit or miss choices (Figure 13F) as well as the variance of population neural coding in V1 and PPC (Figure 19). Therefore, I conclude that the previous rewards cannot solely explain the recruitment of non-sensory neurons in V1 and PPC. On the other hand, it is possible that task-irrelevant movements during task performance could have affected hit responses due to suboptimal head and body positions(Krumin et al., 2018; Musall et al., 2019). However, such behavioral misalignment does not explain the increased noise correlation in V1. This suggests that,

at least, the accurate performance in hit trials is due to an intrinsic population-level

mechanism that can be related to sensory-motor transformation during the task(Pho et al.,

2018), while highlighting the non-trivial contribution of non-sensory neurons in the

process. Although previous studies indicated the significant contributions of non-sensory

neurons to perceptual decision making(Safaai et al., 2013; Leavitt et al., 2017; Insanally

et al., 2019; Zuo and Diamond, 2019), most of them employed sensory categorization

tasks in the forced-choice paradigm, which unavoidably suffers from stimulus uncertainty

causing subjective biases due to value-based decisions. My data support and extend these

findings by showing that, even in the simplest sensory detection task, lacking inherent

stimulus uncertainty and being less contaminated by value-based decisions, non-sensory

neurons in V1 and PPC play a significant role in sensory decisions at the population level.

4   General discussion

Sensory guided decision making is the key aspect of animals' cognitive function for adaptive action selection in various environments. I described that it is not only driven by the sensory information but also non-sensory factors such as subjects' internal state (e.g., choice bias) in the general introduction. Furthermore, I emphasized that unless care is taken to the potential confound of behavioral readout of decision making in the simple Go/Nogo behavioral paradigm, it will lead to a nontrivial misunderstanding of the neuronal mechanism of sensory guided decision making. To overcome such limitations of the previous behavioral paradigm, I set out to introduce a novel visual cue detection task in rats with the aim of measuring neuronal activity correlated with their visually guided decision making coupled with sensory stimulus and internal state. The key innovations were enabling us to quantify the decisions whether a visual signal reached a certain internal detection threshold. This variable visual detection performance is due to the non-sensory factors such as subjective bias (i.e., internal state). By taking advantage of these relatively homogeneous trials with different behavioral responses to identical stimuli (i.e., Hit+ and Miss+), I investigated the neuronal representation of the stimulus and internal state by recording neuronal activities in two visual cortical areas: primary

visual cortex (V1) and posterior parietal cortex (PPC). The key findings of this research are the following: 1) rats often fail to respond to visual stimuli despite the V1 and PPC neurons significantly responded to the visual stimulus. 2) State fluctuation, but not visual responses, correlates with the visually guided decision. 3) Activity of stimulus non-preferring neurons in V1 and PPC contribute to represent the state fluctuation. 4) Stimulus presentation timing relative to state fluctuations in V1 correlates with visually guided decision.

Objective behavioral performance is often contrasted with the capability to use visual information

My behavioral task allowed me to classify the erroneous "no" response to stimulus presence (Miss) as the following two behavior: missed responses with the capability to choose the correct side when forced (Miss+)" and "missed responses without the capability to choose the correct side when forced (Miss−). This behavioral dissection supports the notion that the classically defined miss response is not sufficient to a readout of animals' visually guided decision making to the stimulus presence. Together, neural correlates of Go/Nogo behavior (see general introduction) may also lead the nontrivial confounds to the understanding of the neural mechanisms of decision making and visual

perception.

Armed with an effective task, I was able to record neuronal activity from multiple visual cortical areas in freely moving rats during the task using the electrophysiological recording technique. Beyond demonstrating the classic visual response to task stimuli, my data provided the key findings and raised some important questions as follows.

V1 neurons responded to the stimulus irrespective of either behavioral performance

In my visual cue detection task, rats correctly and significantly guess the visual stimulus position even if they chose the third option (central choice, see chapter 2 in detail). In line with this behavioral result, population activity in V1 and PPC was significantly driven by visual stimulus by decoding the stimulus trials using a support vector machine (SVM) (see Appendix 7.3). This result suggests that not all visual information was being optimally exploited for visually guided decision making during the behavioral task. Interestingly, neuronal activity in V1 was relatively robust to the visual stimulus in Miss- but was at chance level in PPC (see chapter 3). Notably, these results were found only using my behavioral task and different from the results using Go/Nogo paradigm, in that there is no apparent difference between Hit+ and Miss+ in V1 and PPC in my data. Together, the dissociation of firing rate and pattern in visual cortical

area between Hit and Miss reported in previous studies may derive from the neuronal responses in Miss- trials. Future works will need to address the neuronal dissociation between Hit+, Miss+, and Miss- behaviors.

Internal state representation in V1 and PPC.

In my results, even if the visual response is robust in V1 and PPC, behavioral response to the task stimuli fluctuated in trials. This result raised speculation that the non-sensory factors override the visual information resulting in the trial-by-trial fluctuation of the visually guided decision making. These non-sensory factors may contain various internal fluctuations such as the choice bias (Treviño et al., 2020), recent reward history (Hwang et al., 2017, 2019; Hattori et al., 2019), stimulus history (Busse et al., 2011), motivation (Berditchevskaia et al., 2016; Ortiz et al., 2020), arousal (Schriver et al., 2018; de Gee et al., 2020) (see Appendix 7.4), and selective attention (Wimmer et al., 2015), which I define an "internal state" in this study. Supporting this idea, I made a mathematical model to the task performance and found a significant contribution of the previous reward history to explain their behavioral variability. Together, I used a support vector machine (SVM) to classify their behavioral performance (Hit+ vs Miss+) from the pre-stimulus neuronal firing data. I found the significant decoding accuracy of behavioral

performance in pre-stimulus timing, suggesting that non-visual factors including reward history influenced their visually guided decision making. Furthermore, I made a SVM to the visual sensitive neurons and non-sensitive neurons with same procedures respectively. Pre-stimulus decoding accuracy was relatively significant in non-sensitive neurons rather than sensitive neurons in both V1 and PPC, indicating that visual non-sensitive neuron contributes to the visually guided decision by modulating the internal state preceding the stimulus presentation. Future work will require to address what non-sensory factors comprise of this pre-stimulus neuronal dissociation and drive their behavioral variability.

Future direction

In this study, I examined the neuronal representation of the internal state in the visual cortical area and its correlation with visually guided decision making. I found that the visual cortical area represents the non-sensory factors that correlate with a visually guided decision prior to the sensory cue presentation. However, my data could not address what components of internal factors generate the dissociation of behavioral variability (Hit+ and Miss+). In my behavioral data, reward history is one of the significant factors to explain the behavioral variability, but it still lacks the full explanation of behavior. This suggests that various internal factors, including reward history, are mingled with each

other and integrated with external input, resulting in behavioral variability. Therefore,

neuroscience will be required to assess the various internal factors that cannot be observed

directly from behavioral actions. For example, behavioral strategy (e.g., exploration and

exploitation) fluctuates in trial-by-trial, motivation to the task engagement might be

changed with time and trials. These factors should be taken care of in the analysis of

visually guided decision making. In this respect, a model-based approach might play a

key role in analyzing such internal factors. Generalized linear model (GLM) and hidden

Markov model (HMM) is one example to model the subject's task strategy, and some

studies have demonstrated that mathematically and accurately describe the subject's

behavior using a mixture of GLM and HMM (Calhoun et al., 2019; Ashwood et al., 2021;

Bolkan et al., 2021). The key innovation of these works is to quantify the switching of

the behavioral strategy to the trial-by-trial task engagement. Future works will need to

classify more in-depth internal factors using the model or devising the quantitative

innovative task design.

Furthermore, it is essential to identify the neural source of internal factors. For

example, arousal and motivation are slow drifted internal factors that covaried with pupil

diameter (Bradley et al., 2008; Schriver et al., 2018; Wang et al., 2018; Cowley et al.,

2020; de Gee et al., 2020; Ortiz et al., 2020). This slow drift is thought to be derived from

the release of neuromodulators throughout the brain. Accumulating works reported that norepinephrine, the locus coeruleus (LC) released to many different brain areas (Aston-Jones and Cohen, 2005; Sara, 2009; Sara and Bouret, 2012; Poe et al., 2020), and acetylcholine, the basal forebrain released to the multiple brain areas (Villano et al., 2017; Yüzgeç et al., 2018), are thought to be a strong candidate to manipulate the slow drifted internal state. Experimentally, optogenetic manipulation of the acetylcholine imposed the pupil diameter, which is correlated with the subject's arousal. Future work will need to address the relationship between direct manipulation of these neuromodulators and visually guided decision making.

On the other hand, it is essential to address how the internal state influences the neuronal processes that encode the external input and drive the behavioral variability. My data shows that population encoding of the visual stimulus is orthogonally embedded to the internal state fluctuations. This indicates that these two factors are not integrated directly, at least in the visual cortical area. In this view, the internal factor (observed in my study) does not function to manipulate the gain control of external input because the stimulus response was not different between Hit+ and Miss+. This leads to speculation that function of the internal factor to the decision making has two hypotheses; internal factor and external input are integrated with each other in higher cortical area than visual

cortical area, or the internal factor influenced directly to the decision process without the interruption of the encoding of external input. Future work will address the encoding architecture in the higher cortical area during the visually guided decision making and direct inhibition of the neuronal activity in the higher cortical area using optogenetic manipulation.

In closing, the internal factor is the non-trivial information to our sensory guided decision making, and my study indicated that the visual cortical area represents it independent of the visual information and correlates with rat's decision making. However, it is still enigmatic how the brain processes the internal factor and external input and drives the decision making. Discovering the mechanism of it will help the various aspect of our life, such as the development of therapeutic agents of addiction and the development of the machines that can make human-like judgments. A novel mathematical approach, behavioral paradigm, optogenetic manipulation, and mixed techniques may help us to take a fresh look at data, lead a novel notion, and generate a new general theory to explain how internal factors and external input give rise to our decision making.

5 Reference

Akaishi R, Umeda K, Nagase A, Sakai K (2014) Autonomous mechanism of internal choice estimate underlies decision inertia. Neuron 81:195–206.

Allen WE, Chen MZ, Pichamoorthy N, Tien RH, Pachitariu M, Luo L, Deisseroth K (2019) Thirst regulates motivated behavior through modulation of brainwide neural population dynamics. Science 364:253.

Aoi MC, Mante V, Pillow JW (2020) Prefrontal cortex exhibits multidimensional dynamic encoding during decision-making. Nat Neurosci 23:1410–1420.

Arens-Arad T, Farah N, Ben-Yaish S, Zlotnik A, Zalevsky Z, Mandel Y (2016) Head mounted DMD based projection system for natural and prosthetic visual stimulation in freely moving rats. Sci Rep 6:34873.

Ashwood ZC, Roy NA, Stone IR, The International Brain Laboratory, Urai AE, Churchland AK, Pouget A, Pillow JW (2021) Mice alternate between discrete strategies during perceptual decision-making. bioRxiv:2020.10.19.346353 Available at: https://www.biorxiv.org/content/10.1101/2020.10.19.346353v4 [Accessed January 22, 2022].

Aston-Jones G, Cohen JD (2005) An integrative theory of locus coeruleus-norepinephrine function: adaptive gain and optimal performance. Annu Rev Neurosci 28:403–450.

Banerjee A, Parente G, Teutsch J, Lewis C, Voigt FF, Helmchen F (2020) Value-guided remapping of sensory cortex by lateral orbitofrontal cortex. Nature 585:245–250.

Berditchevskaia A, Cazé RD, Schultz SR (2016) Performance in a GO/NOGO perceptual task reflects a balance between impulsive and instrumental components of behaviour. Sci Rep 6:27389.

Blake R, Logothetis NK (2002) Visual competition. Nat Rev Neurosci 3:13–21.

Bolkan SS, Stone IR, Pinto L, Ashwood ZC, Iravedra Garcia JM, Herman AL, Singh P, Bandi A, Cox J, Zimmerman CA, Cho JR, Engelhard B, Koay SA, Pillow JW, Witten IB (2021) Strong and opponent contributions of dorsomedial striatal

pathways to behavior depends on cognitive demands and task strategy. bioRxiv:2021.07.23.453573 Available at: https://www.biorxiv.org/content/10.1101/2021.07.23.453573v1 [Accessed January 22, 2022].

Bradley MM, Miccoli L, Escrig MA, Lang PJ (2008) The pupil as a measure of emotional arousal and autonomic activation. Psychophysiology 45:602–607.

Brown EK, Templer VL, Hampton RR (2017) An assessment of domain-general metacognitive responding in rhesus monkeys. Behav Processes 135:132–144.

Busse L, Ayaz A, Dhruv NT, Katzner S, Saleem AB, Schölvinck ML, Zaharia AD, Carandini M (2011) The detection of visual contrast in the behaving mouse. J Neurosci 31:11351–11361.

Calhoun AJ, Pillow JW, Murthy M (2019) Unsupervised identification of the internal states that shape natural behavior. Nat Neurosci 22:2040–2049.

Campion J (1983) Is blindsight an effect of scattered light, spared cortex, and near-threshold vision? Behav Brain Sci 6:423–486.

Carandini M, Churchland AK (2013) Probing perceptual decisions in rodents. Nat Neurosci 16:824–831.

Cardin JA, Palmer LA, Contreras D (2007) Stimulus feature selectivity in excitatory and inhibitory neurons in primary visual cortex. J Neurosci 27:10333–10344.

Christopher M, Sean DK (2006) On the demonstration of blindsight in monkeys. Mind Lang 21:475–483.

Cowey A, Stoerig P (1995) Blindsight in monkeys. Nature 373:247–249.

Cowley BR, Snyder AC, Acar K, Williamson RC, Yu BM, Smith MA (2020) Slow Drift of Neural Activity as a Signature of Impulsivity in Macaque Visual and Prefrontal Cortex. Neuron 108:551-567.e8.

Criaud M, Boulinguez P (2013) Have we been asking the right questions when assessing response inhibition in go/no-go tasks with fMRI? A meta-analysis and critical review. Neurosci Biobehav Rev 37:11–23.

Critchley ID, Rolls ET (n.d.) Hunger and Satiety Modify the Responses of Olfactory and

Visual Neurons in the Primate Orbitofkontal Cortex.

Daw ND, O'Doherty JP, Dayan P, Seymour B, Dolan RJ (2006) Cortical substrates for exploratory decisions in humans. Nature 441:876–879.

de Gee JW, Tsetsos K, Schwabe L, Urai AE, McCormick D, McGinley MJ, Donner TH (2020) Pupil-linked phasic arousal predicts a reduction of choice bias across species and decision domains. Elife 9:e54014.

de Lafuente V, Jazayeri M, Shadlen MN (2015) Representation of accumulating evidence for a decision in two parietal areas. J Neurosci 35:4306–4318.

Dehaene S, Changeux J-P (2011) Experimental and theoretical approaches to conscious processing. Neuron 70:200–227.

Del Cul A, Baillet S, Dehaene S (2007) Brain dynamics underlying the nonlinear threshold for access to consciousness. PLoS Biol 5:e260.

Driscoll LN, Pettit NL, Minderer M, Chettih SN, Harvey CD (2017) Dynamic Reorganization of Neuronal Activity Patterns in Parietal Cortex. Cell 170:986-999.e16.

Fan Y, Gold JI, Ding L (2018) Ongoing, rational calibration of reward-driven perceptual biases. Elife 7 Available at: http://dx.doi.org/10.7554/eLife.36018.

Foote AL, Crystal JD (2007) Metacognition in the rat. Curr Biol 17:551–555.

Foote AL, Crystal JD (2012) "Play it Again": a new method for testing metacognition in animals. Anim Cogn 15:187–199.

Freedman DJ, Assad JA (2006) Experience-dependent representation of visual categories in parietal cortex. Nature 443:85–88.

Fritsche M, Mostert P, de Lange FP (2017) Opposite Effects of Recent History on Perception and Decision. Curr Biol 27:590–595.

Gail A, Andersen RA (2006) Neural dynamics in monkey parietal reach region reflect context-specific sensorimotor transformations. J Neurosci 26:9376–9384.

Geldard FA, Sherrick CE (1972) The cutaneous "rabbit": a perceptual illusion. Science 178:178–179.

Glickfeld LL, Histed MH, Maunsell JHR (2013) Mouse primary visual cortex is used to detect both orientation and contrast changes. J Neurosci 33:19416–19422.

Goard MJ, Pho GN, Woodson J, Sur M (2016) Distinct roles of visual, parietal, and frontal motor cortices in memory-guided sensorimotor decisions. Elife 5 Available at: http://dx.doi.org/10.7554/eLife.13764.

Goebel R, Muckli L, Zanella FE, Singer W, Stoerig P (2001) Sustained extrastriate cortical activation without visual awareness revealed by fMRI studies of hemianopic patients. Vision Res 41:1459–1474.

Gold JI, Law C-T, Connolly P, Bennur S (2008) The relative influences of priors and sensory evidence on an oculomotor decision variable during perceptual learning. J Neurophysiol 100:2653–2668.

Gold JI, Shadlen MN (2007) The neural basis of decision making. Annu Rev Neurosci 30:535–574.

Goldbach HC, Akitake B, Leedy CE, Histed MH (2021) Performance in even a simple perceptual task depends on mouse secondary visual areas. Elife 10:e62156.

Green DM, Swets JA, Others (1966) Signal detection theory and psychophysics. Wiley New York.

Hangya B, Sanders JI, Kepecs A (2016) A Mathematical Framework for Statistical Decision Confidence. Neural Comput 28:1840–1858.

Hanks TD, Kopec CD, Brunton BW, Duan CA, Erlich JC, Brody CD (2015) Distinct relationships of parietal and prefrontal cortices to evidence accumulation. Nature 520:220–223.

Harris KD, Hirase H, Leinekugel X, Henze DA, Buzsáki G (2001) Temporal interaction between single spikes and complex spike bursts in hippocampal pyramidal cells. Neuron 32:141–149.

Harris KD, Thiele A (2011) Cortical state and attention. Nat Rev Neurosci 12:509–523.

Harvey CD, Coen P, Tank DW (2012) Choice-specific sequences in parietal cortex during a virtual-navigation decision task. Nature 484:62–68.

Hattori R, Danskin B, Babic Z, Mlynaryk N, Komiyama T (2019) Area-Specificity and

Plasticity of History-Dependent Value Coding During Learning. Cell 177:1858-1872.e15.

Hirokawa J, Bosch M, Sakata S, Sakurai Y, Yamamori T (2008) Functional role of the secondary visual cortex in multisensory facilitation in rats. Neuroscience 153:1402–1417.

Hirokawa J, Sadakane O, Sakata S, Bosch M, Sakurai Y, Yamamori T (2011) Multisensory information facilitates reaction speed by enlarging activity difference between superior colliculus hemispheres in rats. PLoS One 6:e25283.

Hirokawa J, Vaughan A, Masset P, Ott T, Kepecs A (2019) Frontal cortex neuron types categorically encode single decision variables. Nature 576:446–451.

Hishida R, Horie M, Tsukano H, Tohmi M, Yoshitake K, Meguro R, Takebayashi H, Yanagawa Y, Shibuki K (2019) Feedback inhibition derived from the posterior parietal cortex regulates the neural properties of the mouse visual cortex. Eur J Neurosci 50:2970–2987.

Histed MH, Carvalho LA, Maunsell JHR (2012) Psychophysical measurement of contrast sensitivity in the behaving mouse. J Neurophysiol 107:758–765.

Hubel DH, Wiesel TN (1959) Receptive fields of single neurones in the cat's striate cortex. J Physiol 148:574–591.

Hubel DH, Wiesel TN (1962) Receptive fields, binocular interaction and functional architecture in the cat's visual cortex. J Physiol 160:106–154.

Hubel DH, Wiesel TN (1963) Shape and arrangement of columns in cat's striate cortex. J Physiol 165:559–568.

Hubel DH, Wiesel TN (1974) Sequence regularity and geometry of orientation columns in the monkey striate cortex. J Comp Neurol 158:267–293.

Humphrey NK (1974) Vision in a monkey without striate cortex: a case study. Perception 3:241–255.

Hwang EJ, Dahlen JE, Mukundan M, Komiyama T (2017) History-based action selection bias in posterior parietal cortex. Nat Commun 8:1242.

Hwang EJ, Link TD, Hu YY, Lu S, Wang EH-J, Lilascharoen V, Aronson S, O'Neil K,

Lim BK, Komiyama T (2019) Corticostriatal Flow of Action Selection Bias. Neuron 104:1126-1140.e6.

Ibos G, Freedman DJ (2017) Sequential sensory and decision processing in posterior parietal cortex. Elife 6:e23743.

Insanally MN, Carcea I, Field RE, Rodgers CC, DePasquale B, Rajan K, DeWeese MR, Albanna BF, Froemke RC (2019) Spike-timing-dependent ensemble encoding by non-classically responsive cortical neurons. Elife 8 Available at: http://dx.doi.org/10.7554/eLife.42409.

Jacobs EAK, Steinmetz NA, Peters AJ, Carandini M, Harris KD (2020) Cortical State Fluctuations during Sensory Decision Making. Curr Biol 30:4944-4955.e7.

Jasper AI, Tanabe S, Kohn A (2019) Predicting Perceptual Decisions Using Visual Cortical Population Responses and Choice History. J Neurosci 39:6714–6727.

Jozefowiez J, Staddon JER, Cerutti DT (2009) Metacognition in animals: how do we know that they know? Comp Cogn Behav Rev 4 Available at: http://comparative-cognition-and-behavior-reviews.org/2009/vol4_jozefowiez_staddon_cerutti_a/.

Kanai R, Muggleton NG, Walsh V (2008) TMS over the intraparietal sulcus induces perceptual fading. J Neurophysiol 100:3343–3350.

Kanai R, Tsuchiya N, Verstraten FAJ (2006) The scope and limits of top-down attention in unconscious visual processing. Curr Biol 16:2332–2336.

Kanai R, Walsh V, Tseng C-H (2010) Subjective discriminability of invisibility: a framework for distinguishing perceptual and attentional failures of awareness. Conscious Cogn 19:1045–1057.

Keeley SL, Zoltowski DM, Aoi MC, Pillow JW (2020) Modeling statistical dependencies in multi-region spike train data. Curr Opin Neurobiol 65:194–202.

Keller AJ, Roth MM, Scanziani M (2020) Feedback generates a second receptive field in neurons of the visual cortex. Nature 582:545–549.

Keller GB, Bonhoeffer T, Hübener M (2012) Sensorimotor mismatch signals in primary visual cortex of the behaving mouse. Neuron 74:809–815.

Kepecs A, Mainen ZF (2012) A computational framework for the study of confidence in

humans and animals. Philos Trans R Soc Lond B Biol Sci 367:1322–1337.

Kepecs A, Uchida N, Zariwala HA, Mainen ZF (2008) Neural correlates, computation and behavioural impact of decision confidence. Nature 455:227–231.

Kim C-Y, Blake R (2005) Psychophysical magic: rendering the visible "invisible." Trends Cogn Sci 9:381–388.

Kimura R, Saiki A, Fujiwara-Tsukamoto Y, Ohkubo F, Kitamura K, Matsuzaki M, Sakai Y, Isomura Y (2012) Reinforcing operandum: rapid and reliable learning of skilled forelimb movements by head-fixed rodents. J Neurophysiol 108:1781–1792.

Koch C, Ullman S (1985) Shifts in selective visual attention: towards the underlying neural circuitry. Hum Neurobiol 4:219–227.

Kolb FC, Braun J (1995) Blindsight in normal observers. Nature 377:336–338.

Krumin M, Lee JJ, Harris KD, Carandini M (2018) Decision and navigation in mouse parietal cortex. Elife 7 Available at: http://dx.doi.org/10.7554/eLife.42583.

Lak A, Costa GM, Romberg E, Koulakov AA, Mainen ZF, Kepecs A (2014) Orbitofrontal cortex is required for optimal waiting based on decision confidence. Neuron 84:190–201.

Lak A, Nomoto K, Keramati M, Sakagami M, Kepecs A (2017) Midbrain Dopamine Neurons Signal Belief in Choice Accuracy during a Perceptual Decision. Curr Biol 27:821–832.

Lak A, Okun M, Moss MM, Gurnani H, Farrell K, Wells MJ, Reddy CB, Kepecs A, Harris KD, Carandini M (2020) Dopaminergic and Prefrontal Basis of Learning from Sensory Confidence and Reward Value. Neuron 105:700-711.e6.

Lampl I, Anderson JS, Gillespie DC, Ferster D (2001) Prediction of orientation selectivity from receptive field architecture in simple cells of cat visual cortex. Neuron 30:263–274.

Lauritzen TZ, Miller KD (2003) Different roles for simple-cell and complex-cell inhibition in V1. J Neurosci 23:10201–10213.

Leavitt ML, Pieper F, Sachs AJ, Martinez-Trujillo JC (2017) Correlated variability modifies working memory fidelity in primate prefrontal neuronal ensembles. Proc

Natl Acad Sci U S A 114:E2494–E2503.

Li N, Daie K, Svoboda K, Druckmann S (2016) Robust neuronal dynamics in premotor cortex during motor planning. Nature 532:459–464.

Licata AM, Kaufman MT, Raposo D, Ryan MB, Sheppard JP, Churchland AK (2017) Posterior Parietal Cortex Guides Visual Decisions in Rats. J Neurosci 37:4954–4966.

Mante V, Sussillo D, Shenoy KV, Newsome WT (2013) Context-dependent computation by recurrent dynamics in prefrontal cortex. Nature 503:78–84.

Marques T, Nguyen J, Fioreze G, Petreanu L (2018) The functional organization of cortical feedback inputs to primary visual cortex. Nat Neurosci 21:757–764.

Masset P, Ott T, Lak A, Hirokawa J, Kepecs A (2020) Behavior- and Modality-General Representation of Confidence in Orbitofrontal Cortex. Cell 182:112-126.e18.

McGurk H, MacDonald J (1976) Hearing lips and seeing voices. Nature 264:746–748.

Meier P, Reinagel P (2011) Rat performance on visual detection task modeled with divisive normalization and adaptive decision thresholds. J Vis 11 Available at: http://dx.doi.org/10.1167/11.9.1.

Merikle PM, Smilek D, Eastwood JD (2001) Perception without awareness: perspectives from cognitive psychology. Cognition 79:115–134.

Monier C, Chavane F, Baudot P, Graham LJ, Frégnac Y (2003) Orientation and direction selectivity of synaptic inputs in visual cortical neurons: a diversity of combinations produces spike tuning. Neuron 37:663–680.

Monk KJ, Allard S, Hussain Shuler MG (2020) Reward Timing and Its Expression by Inhibitory Interneurons in the Mouse Primary Visual Cortex. Cereb Cortex 30:4662–4676.

Montijn JS, Goltstein PM, Pennartz CMA (2015) Mouse V1 population correlates of visual detection rely on heterogeneity within neuronal response patterns. Elife 4:e10163.

Montijn JS, Meijer GT, Lansink CS, Pennartz CMA (2016) Population-Level Neural Codes Are Robust to Single-Neuron Variability from a Multidimensional Coding

Perspective. Cell Rep 16:2486–2498.

Montijn JS, Vinck M, Pennartz CMA (2014) Population coding in mouse visual cortex: response reliability and dissociability of stimulus tuning and noise correlation. Front Comput Neurosci 8:58.

Monto S, Palva S, Voipio J, Palva JM (2008) Very slow EEG fluctuations predict the dynamics of stimulus detection and oscillation amplitudes in humans. J Neurosci 28:8268–8272.

Morcos AS, Harvey CD (2016) History-dependent variability in population dynamics during evidence accumulation in cortex. Nat Neurosci 19:1672–1681.

Moreno-Bote R, Beck J, Kanitscheider I, Pitkow X, Latham P, Pouget A (2014) Information-limiting correlations. Nat Neurosci 17:1410–1417.

Musall S, Kaufman MT, Juavinett AL, Gluf S, Churchland AK (2019) Single-trial neural dynamics are dominated by richly varied movements. Nat Neurosci 22:1677–1686.

Najafi F, Elsayed GF, Cao R, Pnevmatikakis E, Latham PE, Cunningham JP, Churchland AK (2020) Excitatory and Inhibitory Subnetworks Are Equally Selective during Decision-Making and Emerge Simultaneously during Learning. Neuron 105:165-179.e8.

Newby EA, Rock I (1998) Inattentional blindness as a function of proximity to the focus of attention. Perception 27:1025–1040.

Niell CM, Stryker MP (2010) Modulation of visual responses by behavioral state in mouse visual cortex. Neuron 65:472–479.

Nienborg H, Cumming BG (2014) Decision-related activity in sensory neurons may depend on the columnar architecture of cerebral cortex. J Neurosci 34:3579–3585.

Niv Y, Daw ND, Joel D, Dayan P (2007) Tonic dopamine: opportunity costs and the control of response vigor. Psychopharmacology 191:507–520.

O'Doherty J, Dayan P, Schultz J, Deichmann R, Friston K, Dolan RJ (2004) Dissociable roles of ventral and dorsal striatum in instrumental conditioning. Science 304:452–454.

Ohnuki T, Osako Y, Manabe H, Sakurai Y, Hirokawa J (2020) Dynamic coordination of the perirhinal cortical neurons supports coherent representations between task epochs. Commun Biol 3:406.

Ortiz AV, Aziz D, Hestrin S (2020) Motivation and Engagement during Visually Guided Behavior. Cell Rep 33:108272.

Osako Y, Sakurai Y, Hirokawa J (2018) Subjective decision threshold for accurate visual detection performance in rats. Sci Rep 8:9357.

Osborne LC, Hohl SS, Bialek W, Lisberger SG (2007) Time course of precision in smooth-pursuit eye movements of monkeys. J Neurosci 27:2987–2998.

Overgaard M, Rote J, Mouridsen K, Ramsøy TZ (2006) Is conscious perception gradual or dichotomous? A comparison of report methodologies during a visual task. Conscious Cogn 15:700–708.

Park IM, Meister MLR, Huk AC, Pillow JW (2014) Encoding and decoding in parietal cortex during sensorimotor decision-making. Nat Neurosci 17:1395–1403.

Parker AJ, Newsome WT (1998) Sense and the single neuron: probing the physiology of perception. Annu Rev Neurosci 21:227–277.

Parthasarathy A, Herikstad R, Bong JH, Medina FS, Libedinsky C, Yen S-C (2017) Mixed selectivity morphs population codes in prefrontal cortex. Nat Neurosci 20:1770–1779.

Persaud N, McLeod P (2008) Wagering demonstrates subconscious processing in a binary exclusion task. Conscious Cogn 17:565–575.

Persaud N, McLeod P, Cowey A (2007) Post-decision wagering objectively measures awareness. Nat Neurosci 10:257–261.

Peter UT, Martinez-Conde S, Schlegel AA, Macknik SL (2005) Visibility, visual awareness, and visual masking of simple unattended targets are confined to areas in the occipital cortex beyond human V1/V2. Proceedings of the National Academy of Sciences 102:17178–17183.

Pho GN, Goard MJ, Woodson J, Crawford B, Sur M (2018) Task-dependent representations of stimulus and choice in mouse parietal cortex. Nat Commun 9:2596.

Pillow JW, Shlens J, Paninski L, Sher A, Litke AM, Chichilnisky EJ, Simoncelli EP (2008) Spatio-temporal correlations and visual signalling in a complete neuronal population. Nature 454:995–999.

Platt ML, Glimcher PW (1999) Neural correlates of decision variables in parietal cortex. Nature 400:233–238.

Poe GR, Foote S, Eschenko O, Johansen JP, Bouret S, Aston-Jones G, Harley CW, Manahan-Vaughan D, Weinshenker D, Valentino R, Berridge C, Chandler DJ, Waterhouse B, Sara SJ (2020) Locus coeruleus: a new look at the blue spot. Nat Rev Neurosci 21:644–659.

Ress D, Backus BT, Heeger DJ (2000) Activity in primary visual cortex predicts performance in a visual detection task. Nat Neurosci 3:940–945.

Rumyantsev OI, Lecoq JA, Hernandez O, Zhang Y, Savall J, Chrapkiewicz R, Li J, Zeng H, Ganguli S, Schnitzer MJ (2020) Fundamental bounds on the fidelity of sensory cortical coding. Nature 580:100–105.

Safaai H, von Heimendahl M, Sorando JM, Diamond ME, Maravall M (2013) Coordinated population activity underlying texture discrimination in rat barrel cortex. J Neurosci 33:5843–5855.

Sakata S, Kitsukawa T, Kaneko T, Yamamori T, Sakurai Y (2002) Task-dependent and cell-type-specific Fos enhancement in rat sensory cortices during audio-visual discrimination. Eur J Neurosci 15:735–743.

Sakata S, Yamamori T, Sakurai Y (2004) Behavioral studies of auditory-visual spatial recognition and integration in rats. Exp Brain Res 159:409–417.

Sanders JI, Kepecs A (2014) A low-cost programmable pulse generator for physiology and behavior. Front Neuroeng 7:43.

Sara SJ (2009) The locus coeruleus and noradrenergic modulation of cognition. Nat Rev Neurosci 10:211–223.

Sara SJ, Bouret S (2012) Orienting and reorienting: the locus coeruleus mediates cognition through arousal. Neuron 76:130–141.

Schall JD (2001) Neural basis of deciding, choosing and acting. Nat Rev Neurosci 2:33–42.

Schiller PH (2010) Parallel information processing channels created in the retina. Proc Natl Acad Sci U S A 107:17087–17094.

Schriver BJ, Bagdasarov S, Wang Q (2018) Pupil-linked arousal modulates behavior in rats performing a whisker deflection direction discrimination task. J Neurophysiol 120:1655–1670.

Shadlen MN, Newsome WT (1996) Motion perception: seeing and deciding. Proc Natl Acad Sci U S A 93:628–633.

Shams L, Kamitani Y, Shimojo S (2002) Visual illusion induced by sound. Brain Res Cogn Brain Res 14:147–152.

Shimaoka D, Steinmetz NA, Harris KD, Carandini M (2019) The impact of bilateral ongoing activity on evoked responses in mouse cortex. Elife 8 Available at: http://dx.doi.org/10.7554/eLife.43533.

Shin H, Moore CI (2019) Persistent Gamma Spiking in SI Nonsensory Fast Spiking Cells Predicts Perceptual Success. Neuron 103:1150-1163.e5.

Shuler MG, Bear MF (2006) Reward timing in the primary visual cortex. Science 311:1606–1609.

Silvanto J, Muggleton N, Lavie N, Walsh V (2009) The perceptual and functional consequences of parietal top-down modulation on the visual cortex. Cereb Cortex 19:327–330.

Smallwood J, Schooler JW (2006) The restless mind. Psychol Bull 132:946–958.

Soltani A, Koechlin E (2022) Computational models of adaptive behavior and prefrontal cortex. Neuropsychopharmacology 47:58–71.

Soma S, Suematsu N, Shimegi S (2014) Efficient training protocol for rapid learning of the two-alternative forced-choice visual stimulus detection task. Physiol Rep 2 Available at: http://dx.doi.org/10.14814/phy2.12060.

Somers DC, Nelson SB, Sur M (1995) An emergent model of orientation selectivity in cat visual cortical simple cells. J Neurosci 15:5448–5465.

Speed A, Del Rosario J, Burgess CP, Haider B (2019) Cortical State Fluctuations across Layers of V1 during Visual Spatial Perception. Cell Rep 26:2868-2874.e3.

Stănişor L, van der Togt C, Pennartz CMA, Roelfsema PR (2013) A unified selection signal for attention and reward in primary visual cortex. Proc Natl Acad Sci U S A 110:9136–9141.

Steinmetz NA, Zatka-Haas P, Carandini M, Harris KD (2019) Distributed coding of choice, action and engagement across the mouse brain. Nature 576:266–273.

Stoerig P, Zontanou A, Cowey A (2002) Aware or unaware: assessment of cortical blindness in four men and a monkey. Cereb Cortex 12:565–574.

Sugrue LP, Corrado GS, Newsome WT (2004) Matching behavior and the representation of value in the parietal cortex. Science 304:1782–1787.

Swaminathan SK, Freedman DJ (2012) Preferential encoding of visual categories in parietal cortex compared with prefrontal cortex. Nat Neurosci 15:315–320.

Templer VL, Lee KA, Preston AJ (2017) Rats know when they remember: transfer of metacognitive responding across odor-based delayed match-to-sample tests. Anim Cogn 20:891–906.

Tolhurst DJ, Movshon JA, Dean AF (1983) The statistical reliability of signals in single neurons in cat and monkey visual cortex. Vision Res 23:775–785.

Tong F (2003) Primary visual cortex and visual awareness. Nat Rev Neurosci 4:219–229.

Treviño M, Medina-Coss Y León R, Haro B (2020) Adaptive Choice Biases in Mice and Humans. Front Behav Neurosci 14:99.

Tsuchiya N, Koch C (2005) Continuous flash suppression reduces negative afterimages. Nat Neurosci 8:1096–1101.

van Vugt B, Dagnino B, Vartak D, Safaai H, Panzeri S, Dehaene S, Roelfsema PR (2018) The threshold for conscious report: Signal loss and response bias in visual and frontal cortex. Science 360:537–542.

Villano I, Messina A, Valenzano A, Moscatelli F, Esposito T, Monda V, Esposito M, Precenzano F, Carotenuto M, Viggiano A, Chieffi S, Cibelli G, Monda M, Messina G (2017) Basal Forebrain Cholinergic System and Orexin Neurons: Effects on Attention. Front Behav Neurosci 11:10.

Walker P, Powell DJ (1979) The sensitivity of binocular rivalry to changes in the

nondominant stimulus. Vision Res 19:247–249.

Wang C-A, Baird T, Huang J, Coutinho JD, Brien DC, Munoz DP (2018) Arousal Effects on Pupil Size, Heart Rate, and Skin Conductance in an Emotional Face Task. Front Neurol 9:1029.

Watanabe M, Cheng K, Murayama Y, Ueno K, Asamizuya T, Tanaka K, Logothetis N (2011) Attention but not awareness modulates the BOLD signal in the human V1 during binocular suppression. Science 334:829–831.

Weiskrantz L (1986) Blindsight: A Case Study and Implications. Oxford University Press.

Wimmer RD, Schmitt LI, Davidson TJ, Nakajima M, Deisseroth K, Halassa MM (2015) Thalamic control of sensory selection in divided attention. Nature 526:705–709.

Yang Y, DeWeese MR, Otazu GH, Zador AM (2008) Millisecond-scale differences in neural activity in auditory cortex can drive decisions. Nat Neurosci 11:1262–1263.

Yoshida M, Hafed ZM, Isa T (2017) Informative Cues Facilitate Saccadic Localization in Blindsight Monkeys. Front Syst Neurosci 11:5.

Yoshida M, Isa T (2015) Signal detection analysis of blindsight in monkeys. Sci Rep 5:10755.

Yoshida M, Itti L, Berg DJ, Ikeda T, Kato R, Takaura K, White BJ, Munoz DP, Isa T (2012) Residual attention guidance in blindsight monkeys watching complex natural scenes. Curr Biol 22:1429–1434.

Yoshida M, Takaura K, Kato R, Ikeda T, Isa T (2008) Striate cortical lesions affect deliberate decision and control of saccade: implication for blindsight. J Neurosci 28:10517–10530.

Yuki S, Okanoya K (2017) Rats show adaptive choice in a metacognitive task with high uncertainty. J Exp Psychol Anim Learn Cogn 43:109–118.

Yüzgeç Ö, Prsa M, Zimmermann R, Huber D (2018) Pupil Size Coupling to Cortical States Protects the Stability of Deep Sleep via Parasympathetic Modulation. Curr Biol 28:392-400.e3.

Zhong L, Zhang Y, Duan CA, Deng J, Pan J, Xu N-L (2019) Causal contributions of parietal cortex to perceptual decision-making during stimulus categorization. Nat

Neurosci 22:963–973.

Zhou Y, Freedman DJ (2019) Posterior parietal cortex plays a causal role in perceptual and categorical decisions. Science 365:180–185.

Zuo Y, Diamond ME (2019) Texture Identification by Bounded Integration of Sensory Cortical Signals. Curr Biol 29:1425-1435.e5.

Zylberberg J (2018) The role of untuned neurons in sensory information coding. bioRxiv:134379 Available at: https://www.biorxiv.org/content/10.1101/134379v6 [Accessed January 22, 2022].

6   Figures
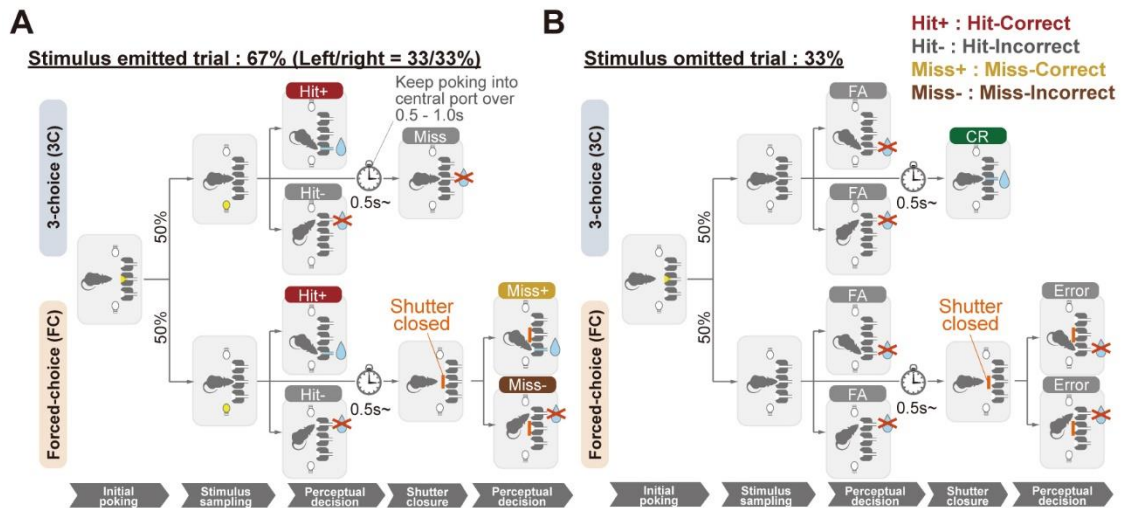
Figure.1 | Visual cue detection task

(A and B) Schematics of the behavioral paradigm. Rats initiated a trial by nose poking into the

central port and waited for 0.2–0.6 s to receive a peripheral stimulus. Rats were rewarded by

poking into the corresponding port when the peripheral stimulus was presented (A) or into the

central port when the stimulus was not presented (B)
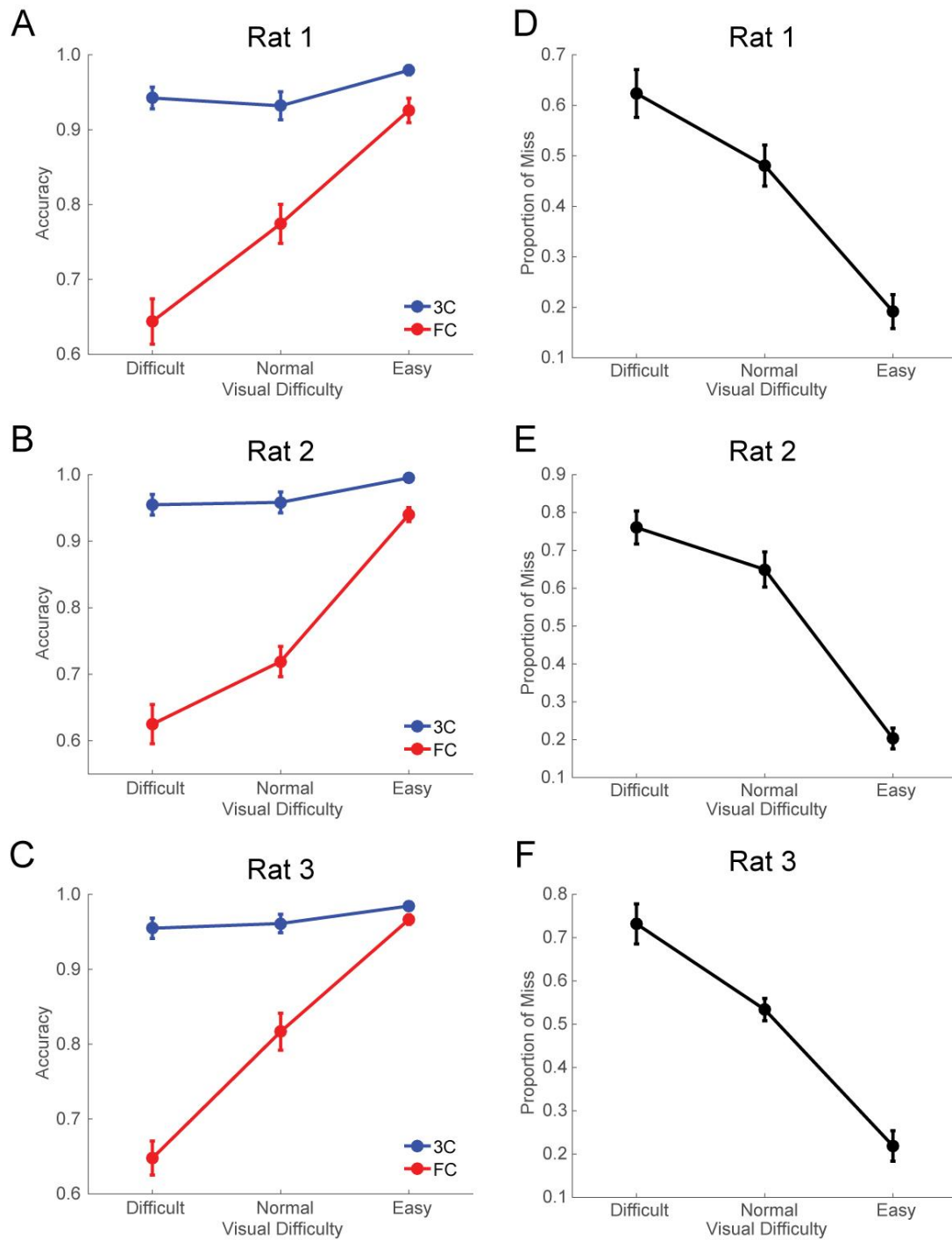
Figure.2 | Behavioral performance in the visual cue detection task.

(A–C) Choice accuracy is shown as mean ± SEM. (D–F) Proportion of misses is shown as

mean ± SEM.
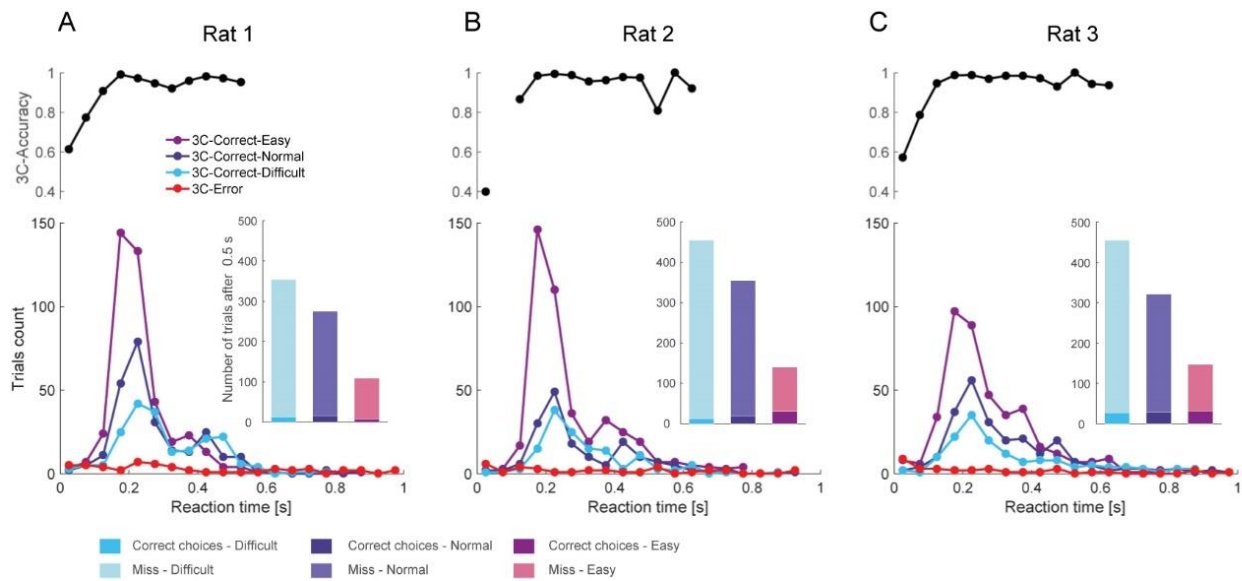
Figure.3 | Reaction time distribution and detection accuracy in the 3C trials.

(A–C) The distributions of reaction times of the spatial choices for correct in three visual difficulty (Easy: purple, Normal: dark blue, Difficult: light blue) and error (red) trials for each subject (bottom). The inset shows the number of correct choices and miss trials with reaction time more than 0.5 s. Spatial choice accuracy for each reaction time bins is shown above (with minimum trial number of 10 trials).
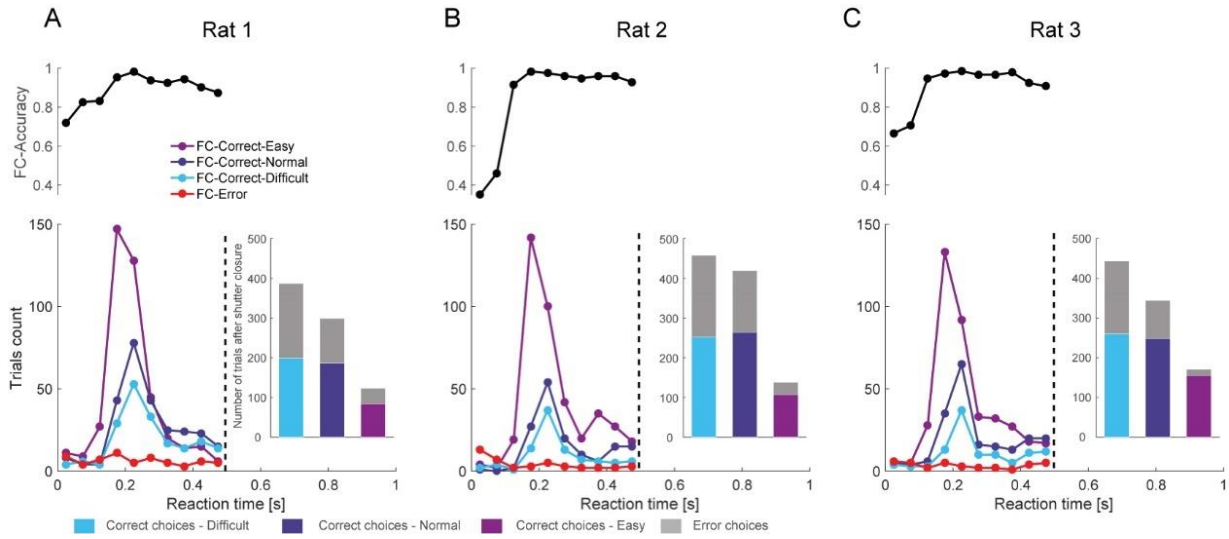
Figure.4 | Reaction time distribution and detection accuracy in the FC trials.

(A–C) The distributions of reaction times of the spatial choices for the correct in three visual difficulty (Easy: purple, Normal: dark blue, Difficult: light blue) and error (red) trials for each subject (bottom). The inset shows the number of correct and error choices after the shutter closure (0.5 s). Spatial choice accuracy for each reaction time bins is shown above (with minimum trial number of 10 trials). Note that only the reaction time before shutter release (<0.5 s) is shown.
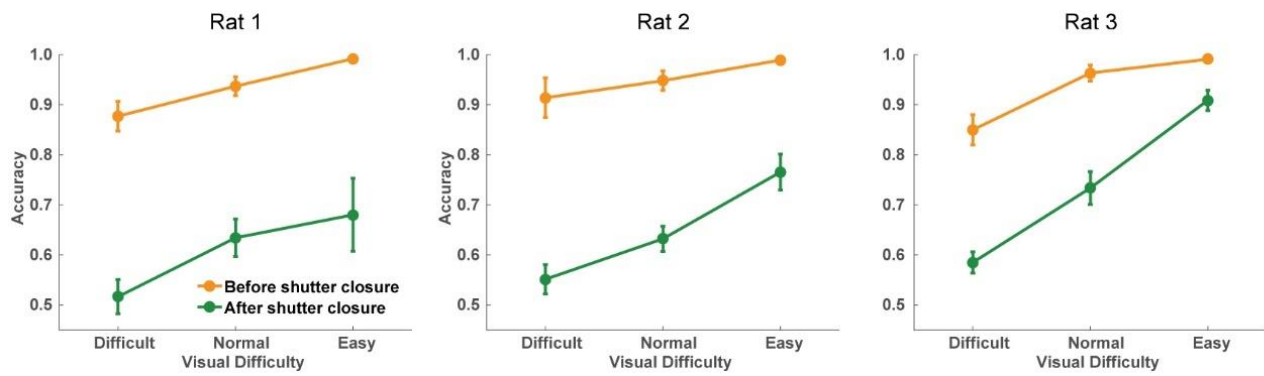
Figure 5 | Choice accuracy of trials after the shutter closure.

Choice accuracy before (green) and after (yellow) the shutter is closed as expressed as mean $\pm$

SEM.
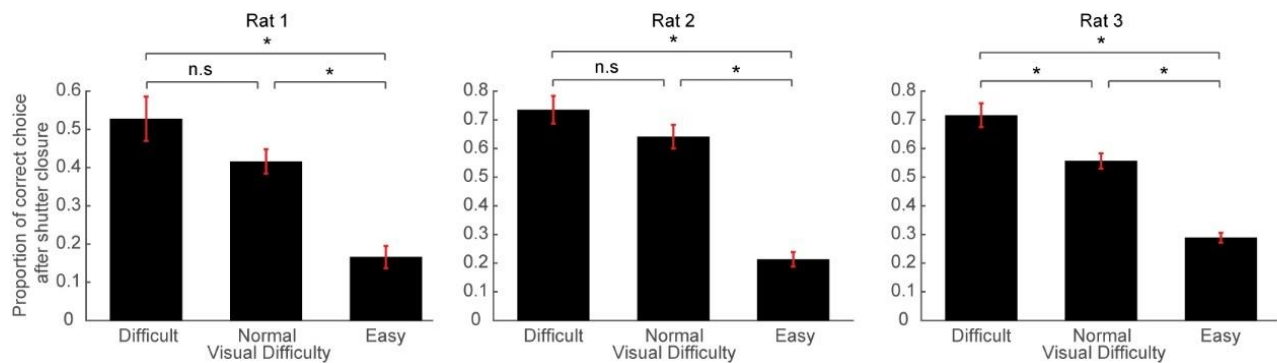
Figure.6 | Proportion of the correct trials after the shutter closure in all the correct trials in FC trials.

Proportion of correct trials after the shutter closure in all correct trials (before and after the shutter closure) is shown as mean $\pm$ SEM. For the analysis of data across conditions, one-way ANOVA and Tukey's test for post-hoc comparison were used. $*p < 0.05$.
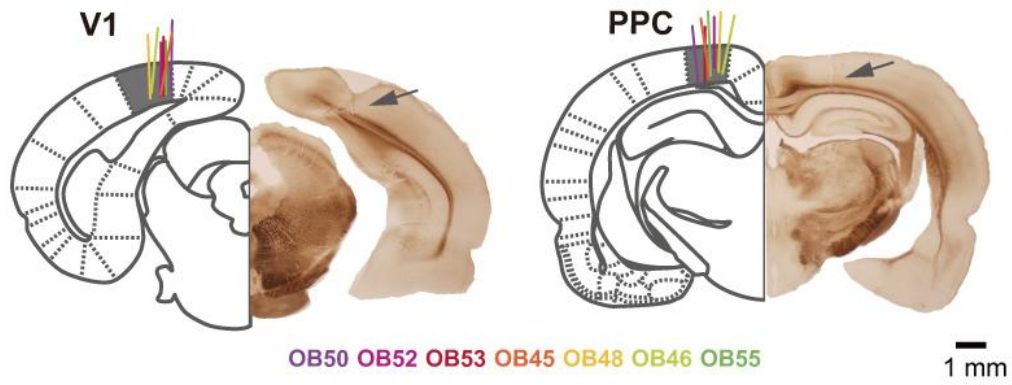
Figure.7 | Recording sites

The coronal section indicating recording sites in V1 and PPC (arrow). We simultaneously recorded neuronal activity in V1 and PPC from seven rats. Each color corresponds to the subject identification number.
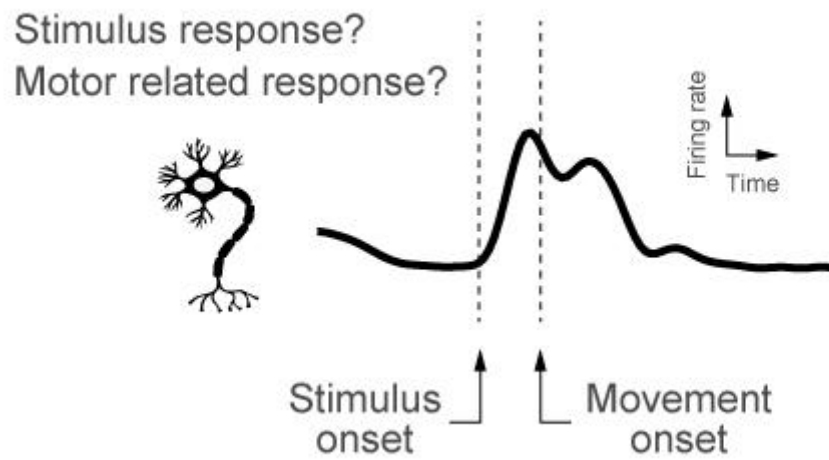
Figure.8 | Example neuron responds to the stimulus and movement

The schematic of the firing rate of an example neuron. In this example, stimulus onset and movement onset are close with time, resulting in the possibility of intermingled neuronal activity based on these two variables.
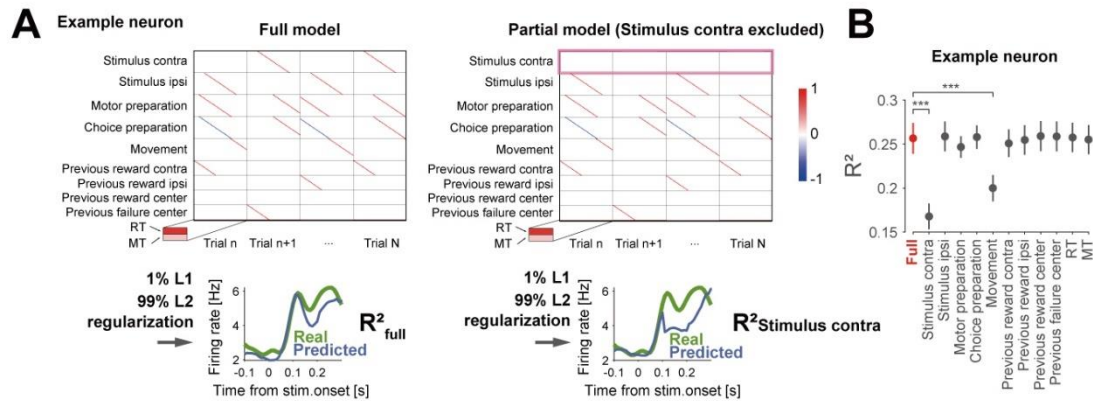
Figure.9 | The procedures of time-locked kernel regression

(A)Structure of predictors (kernels) design matrices. The rows in these matrices represent task

variables (predictors), which can have a -1, 0, or 1 value for time points relative to the appropriate

time offset from the specific task events. In the partial model design matrix, the values of the

target predictor (for example, stimulus contra) were set to zero through the rows (time). Inset,

example fit of individual neurons by using a full model design matrix (left) and a partial model

design matrix where target kernel is contra stimulus (right). Blue and green lines show fitted and

actual data by each model, respectively. (B) Variance explained (tested on held-out data with ten-

fold cross-validation) for each partial model in an example neuron. Partial models were compared

to the full model to determine the selectivity of each kernel (P<0.05, two-sided t-test, Holm-

Bonferroni correction for all model comparison).
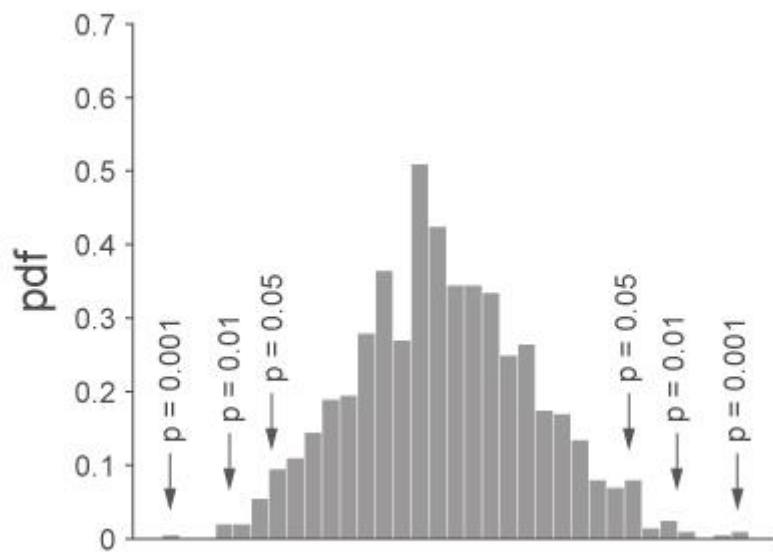
Figure.10 | Statistics

The probability density function of example bootstrapped data (1000 bootstrapped). P-value was

calculated from the percentile of the bootstrapped data. If the empirical data scores in the 97.5%

percentile, the P-value was estimated at 0.05.
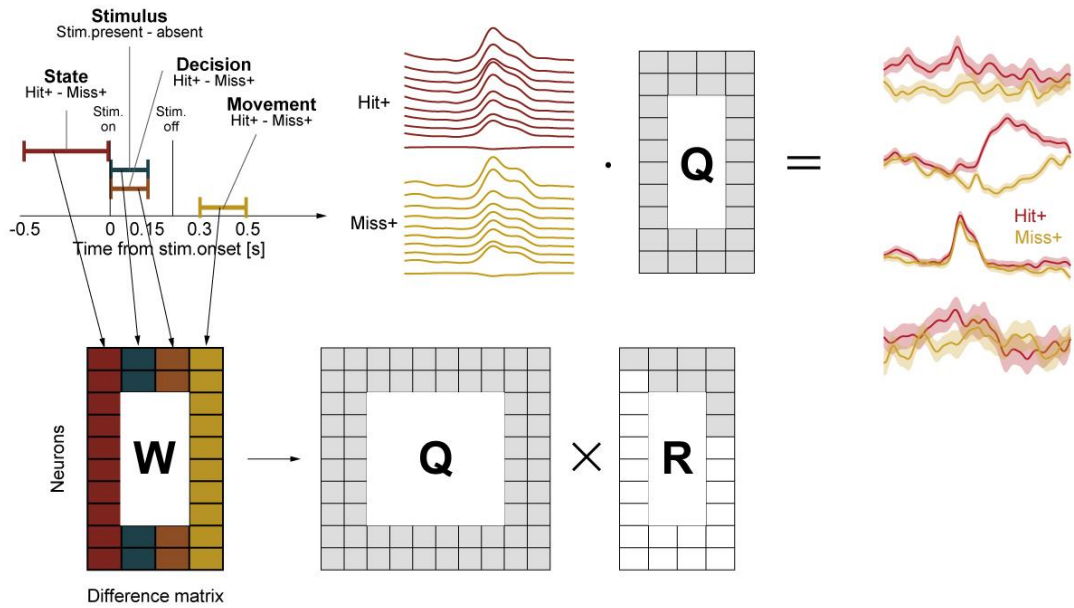
Figure.11 | Schematic of state space analysis at each task and behavioral axis

We constructed the difference matrix W by concatenating the difference of firing rates between

conditions for each epoch. We then obtained the orthogonal axes by orthogonalizing W with the

QR-decomposition. Finally, we draw the population dynamics at each task and behavioral axes

by the dot product of firing rates for each condition (Hit+ and Miss+) and the first four columns

of Q.
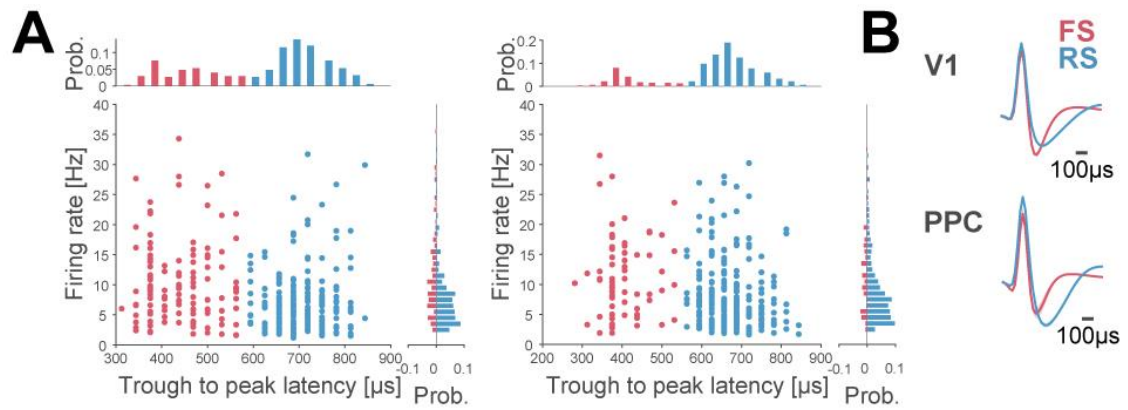
Figure.12 | Cell-type classification

(A) Scatter plot and histograms of the trough to (late) peak latency and firing rates in V1 and PPC.

Each color corresponds to putative fast-spiking (FS) interneurons (pink) and regular-spiking (RS)

neurons (blue). (B) Averaged waveforms of putative FS and RS neurons in V1 and PPC. Shaded

areas show SEM
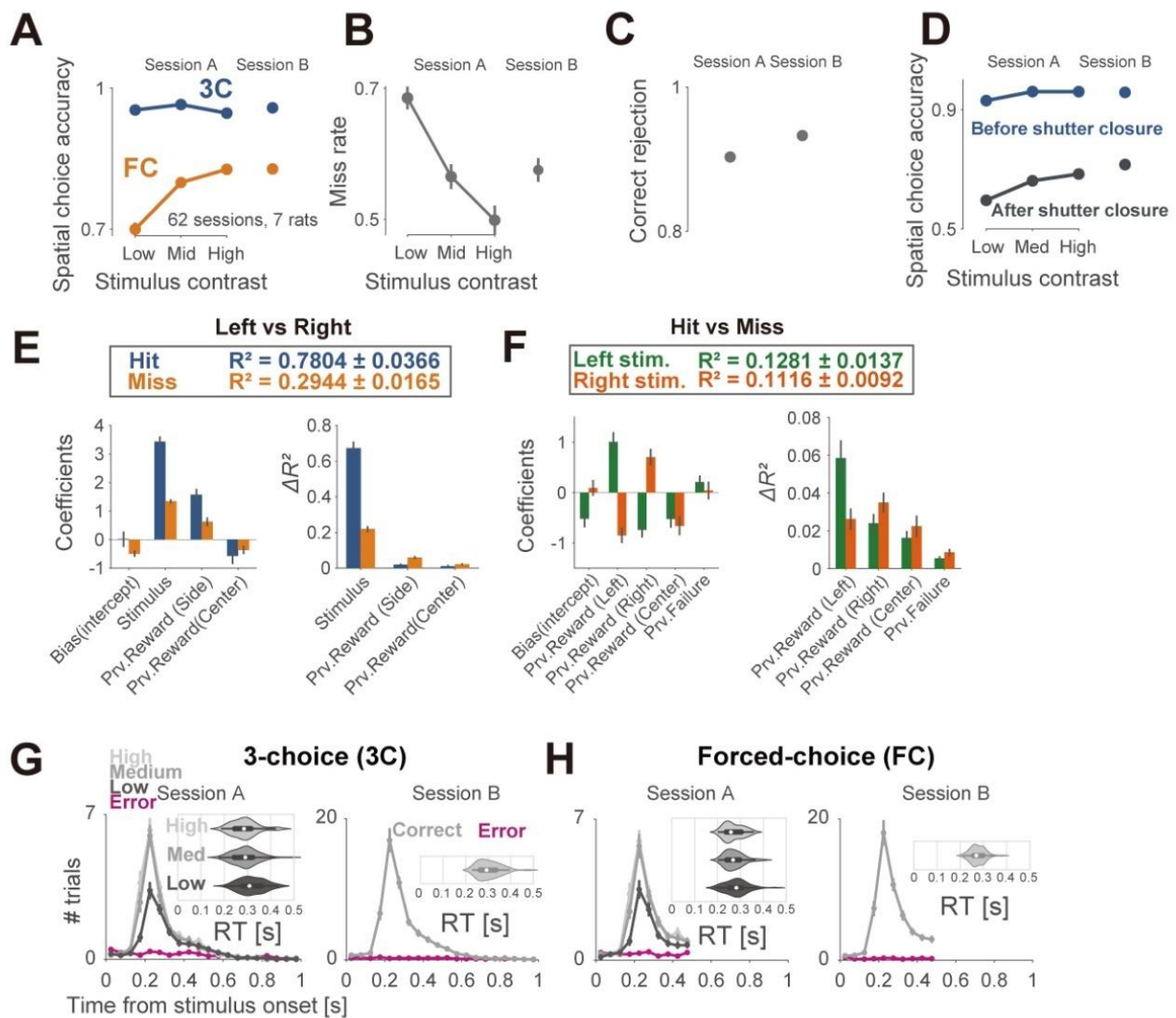
Figure.13 | Behavioral results

(A) Spatial choice accuracy in 3C and FC trials with graded visual contrast in session A and a

fixed contrast in session B. (B) Miss rate in 3C trials. (C) Correct rejection rate in 3C trials. (D)

Spatial choice accuracy before and after shutter closure in FC trials. (E) Impact of task parameters

on behavioral variability using GLM fitting to left or right choice in hit and miss conditions.

Model coefficients in the left panel and the ΔR^2 in the right panel are shown. (F) Impact of task

parameters on behavioral variability using GLM fitting to Left/Right choices in Hit and Miss

response. Model coefficients in the left panel and the ΔR^2 in the right panel. Error bars show

SEM. (G) Distribution of reaction timing in 3C trials of all subjects in session A (left) and B

(right). The colors correspond to visual contrast and error. The inset shows violin plots of reaction

timing for each stimulus contrast. The white circles indicate the median value, and the end of the

thick line quartiles. (H) Same as in G, but in FC trials. Because of shutter closure, reaction timing

was not defined after 0.5 s from stimulus onset.
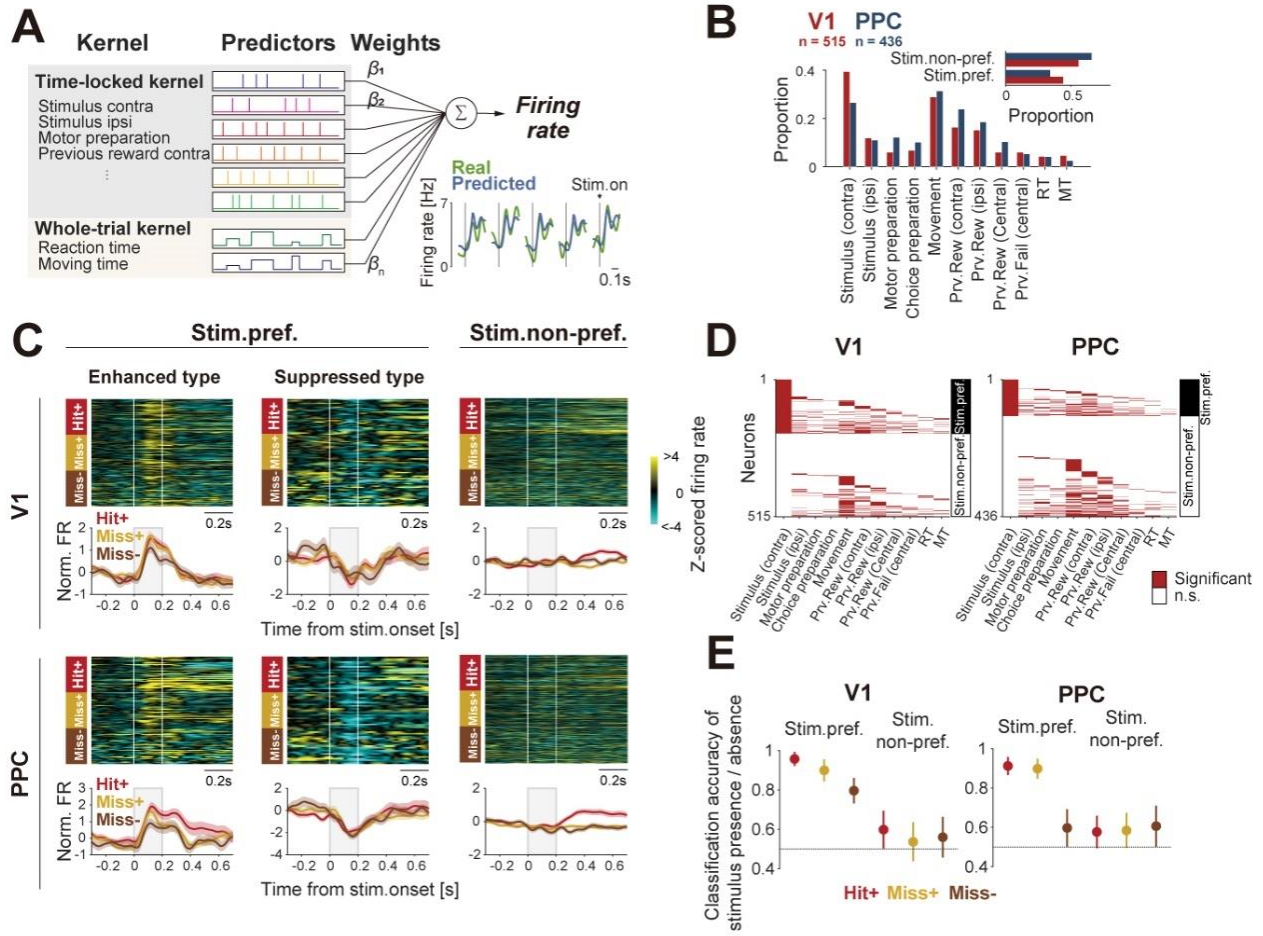
Figure.14 | Quantification of neuronal responses to the task and behavioral variables in V1 and

PPC neurons

(A) Schematic of the encoding model fitted to the neuronal responses to the task and behavioral

variables (see Methods). Inset: real (green) and predicted (blue) firing rates in each cross-

validated dataset are shown. Each vertical line indicates stimulus onset timing. (B) Fraction of

neurons encoding each task and behavioral variable in V1 (red) and PPC (blue). Inset: fraction of

stimulus-preferring and non-preferring neurons in V1 and PPC is shown. (C) Trial-averaged

neuronal activity for each choice outcome in enhanced-type stimulus-preferring neurons (128

V1/74 PPC neurons), suppressed-type stimulus preferring neurons (75 V1/42 PPC neurons), and

stimulus non-preferring neurons (312 V1/320 PPC neurons). Firing rates of all neurons were z-

scored and sorted by max peak latency in Hit+ trials. Shaded area shows SEM. (D) Preferences

of each neuron in V1 and PPC for task and behavioral variables (ordered within stimulus-

preferring and non-preferring neurons). (E) Classification accuracy of predicting the presence of

a contralateral stimulus versus the absence of a stimulus in each choice outcome in stimulus-

preferring and non-preferring population in V1 (top) and PPC (bottom). Error bars show standard

deviation (SD).
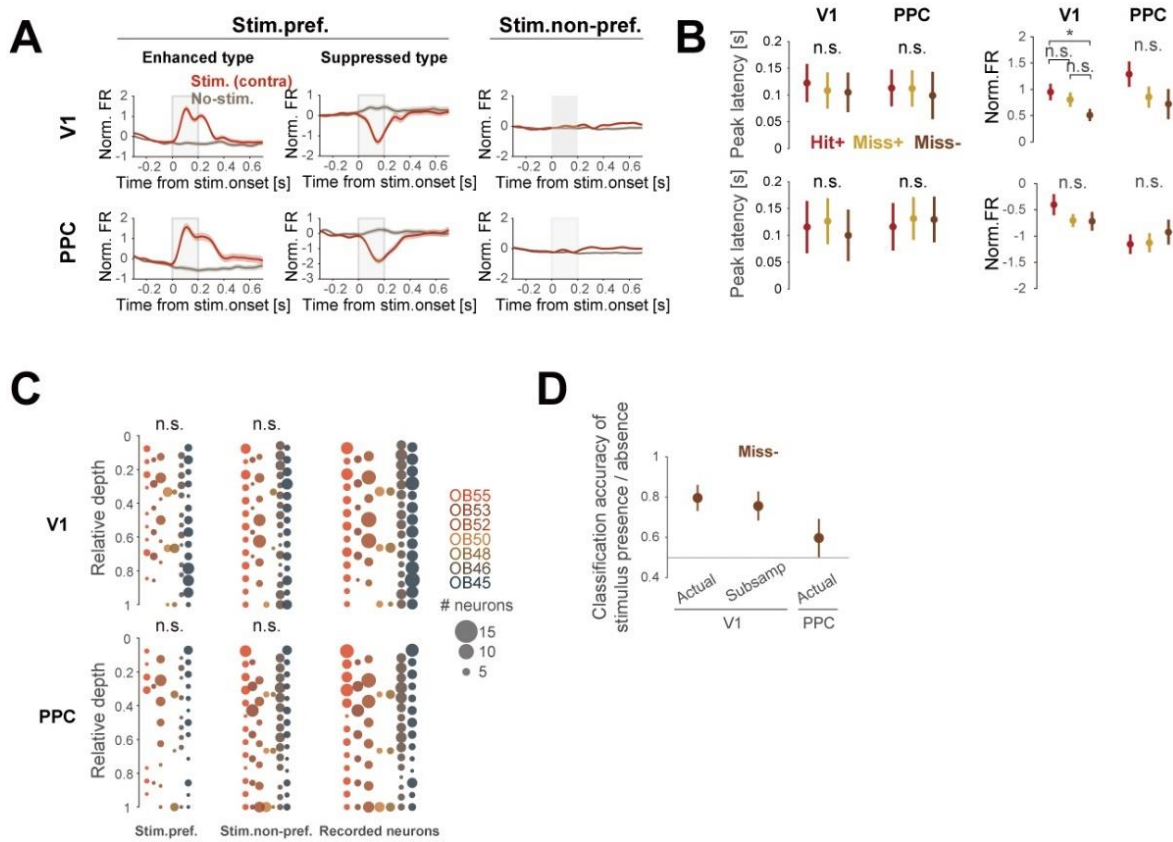
Figure.15 | Firing patterns and spatial distributions in V1 and PPC

(A) Trial averaged firing rates of stimulus encoding (preferring) neurons defined by time-locked

kernel regression (target kernel is stimulus contra) in V1 and PPC aligned to stimulus onset. The

shaded areas show SEM. (B) Peak-latency (left) and firing rate (right) of stimulus preferring

neurons in Enhanced and Suppressed types in each choice type shown as mean ± SEM. (C) Per-

subject recorded neurons in each relative depth (normalized to 0-1 from recording stating point

to end point). The color indicates the subject number, and circle size corresponds to the number

116

of recorded neurons. The Kolmogorov-Smirnov test was used for statistical significance of distributions between all recorded neurons and neuronal subpopulation. (D), Same convention as Figure 5E with identical analysis except that the number of subsampled neurons in V1 was aligned to that of PPC. Error bars show standard deviation (STD).
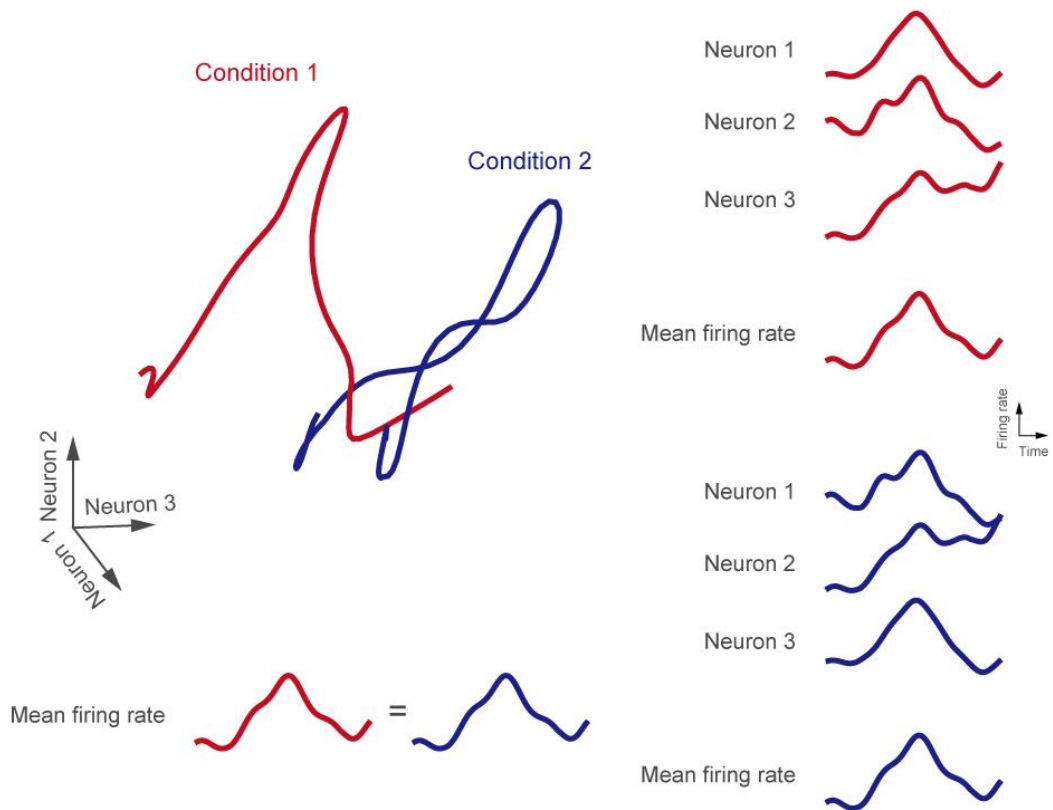
Figure.16 | Difference between mean based and high dimensional metrics

Left, the population activity projecting to the high dimensional neural space in example

conditions 1 and 2. Each axis corresponds to each neural activity. Right, example neuronal

activities in the neurons 1 – 3 in each condition. Mean activity is not different between

conditions, but single neural activity is different between conditions.
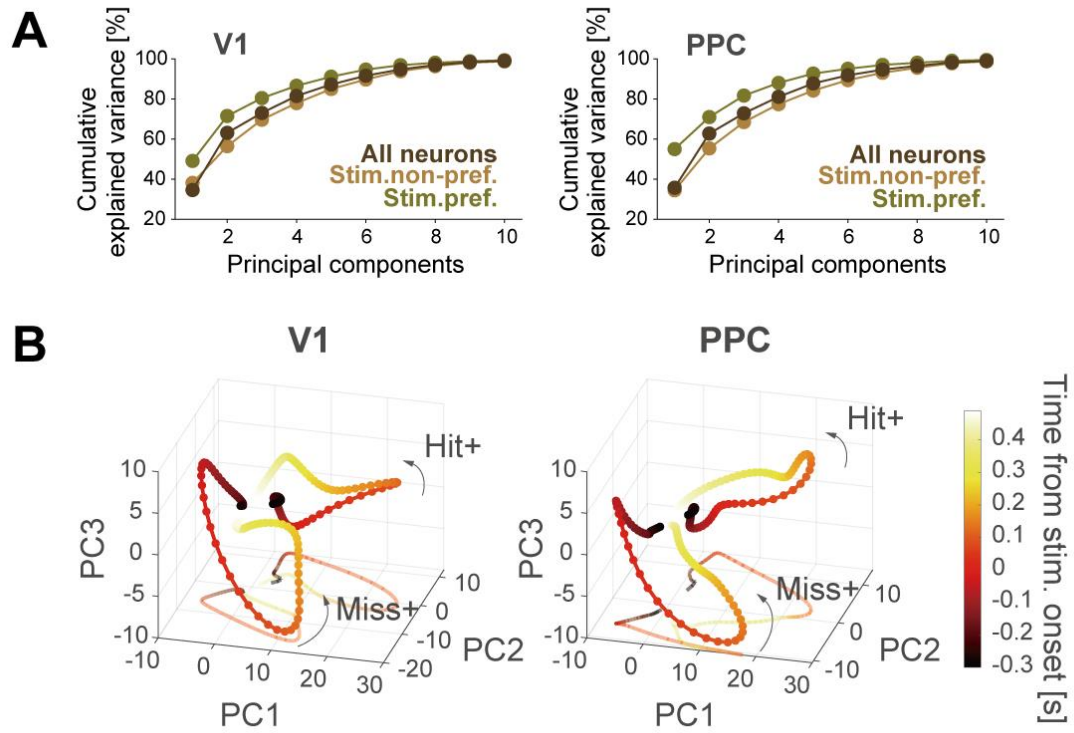
Figure.17 | Explained variance and 3D plot of state space dynamics in V1 and PPC

(A) Cumulative variance explained by the first 10 PCs calculated from the whole, stimulus preferring, and non-preferring population. The variance is calculated over choice types and times.

(B) Population responses of the whole population projected onto three dimensions of the analysis window (-0.1 to 0.15 s from stimulus onset) in V1 and PPC. Each color corresponds to time relative to stimulus onset.
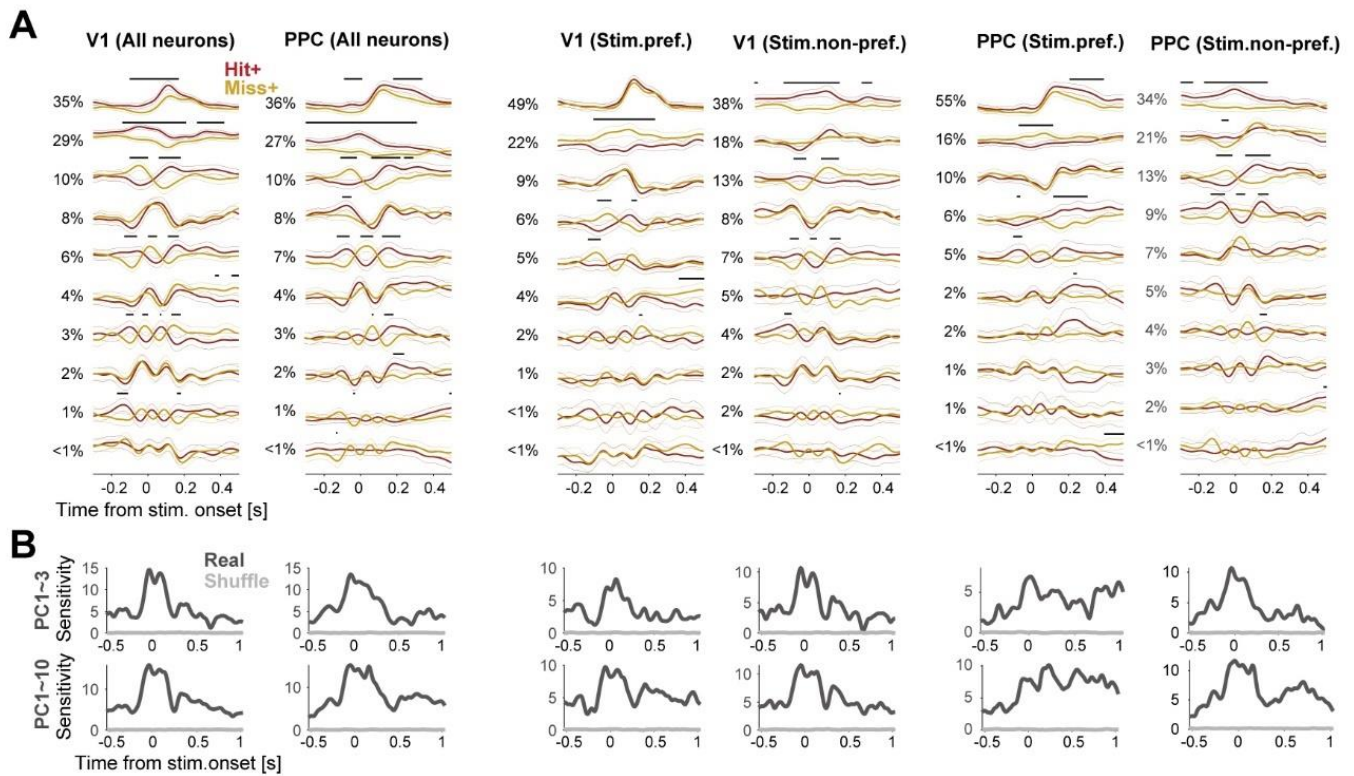
Figure.18 | Pre-stimulus population dynamics and stimulus subspaces in V1 and PPC

(A) PC projections for each choice type in all neurons, stimulus preferring and non-preferring population in V1 and PPC. The thin lines show the 95% percentile. The numbers indicate the explained variances for each principal component. (B) Sensitivity index (d') across choice types computed from the top 3 PCs (top) and top 10 PCs (bottom) in the different time windows for V1 and PPC.
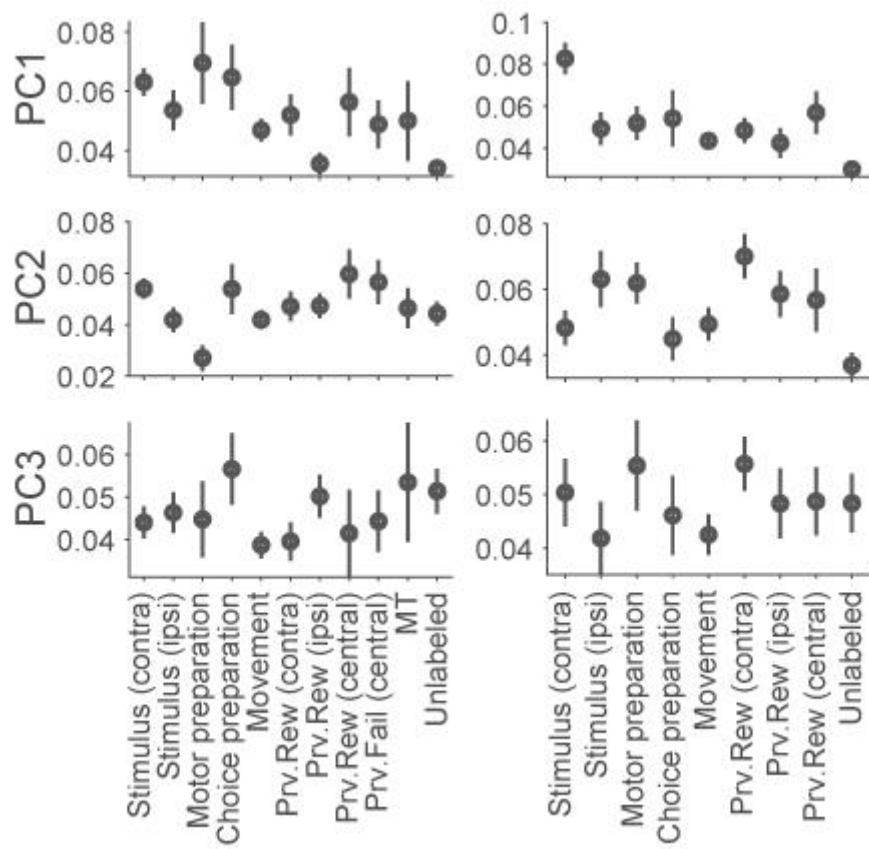
Figure.19 | Weight value in each PC in V1 and PPC

Absolute weight value in each PC shown as mean ± SEM
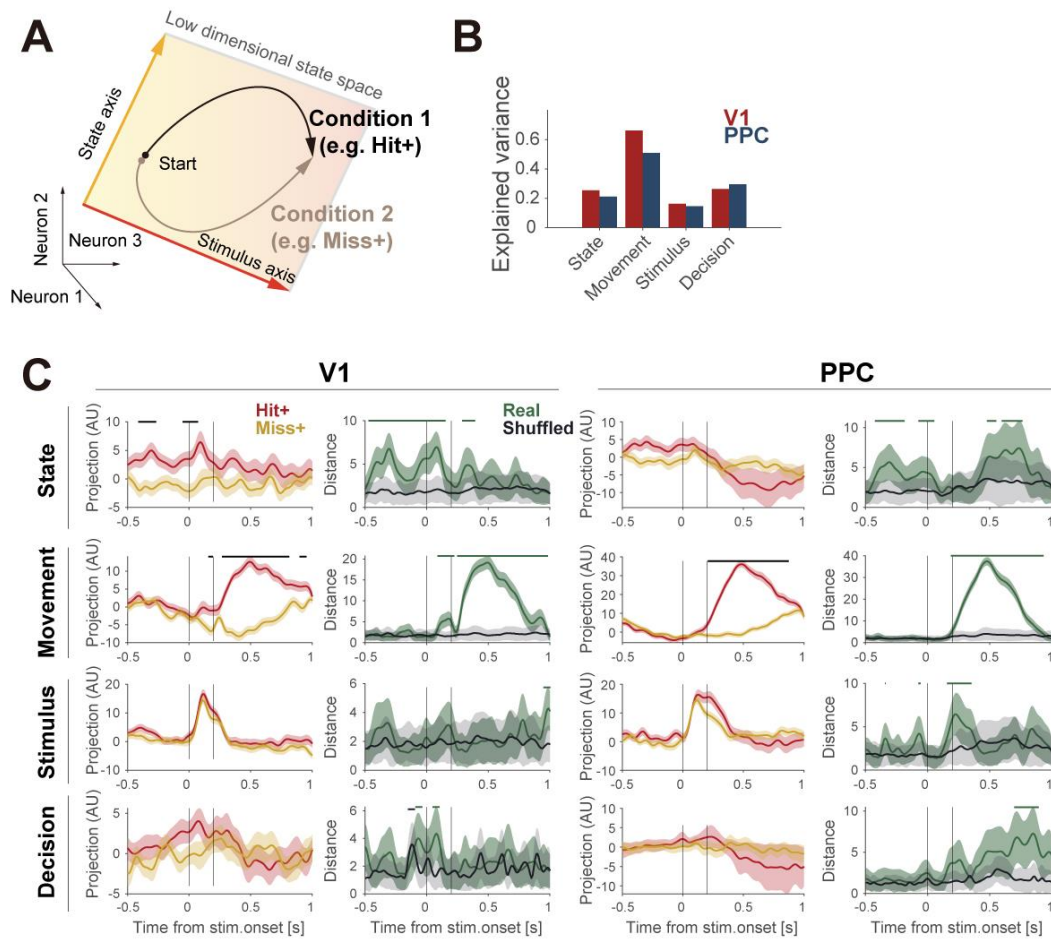
Figure.20 | State dynamics regulation in V1 and PPC

(A) Population dynamics encode the two task-related variables (e.g., state and stimulus) within

the two-dimensional neuronal subspace. (B) Explained variance of each neuronal mode in original

population dynamics in V1 and PPC. Note that the sign of the projections is arbitrary. The distance

of projections is shown for comparison between V1 and PPC. (C) Neuronal projections in each

mode individually in V1 and PPC. Right panels in each V1 and PPC show the distance between

projections in Hit+ and Miss+ trials. Shaded area shows the SD
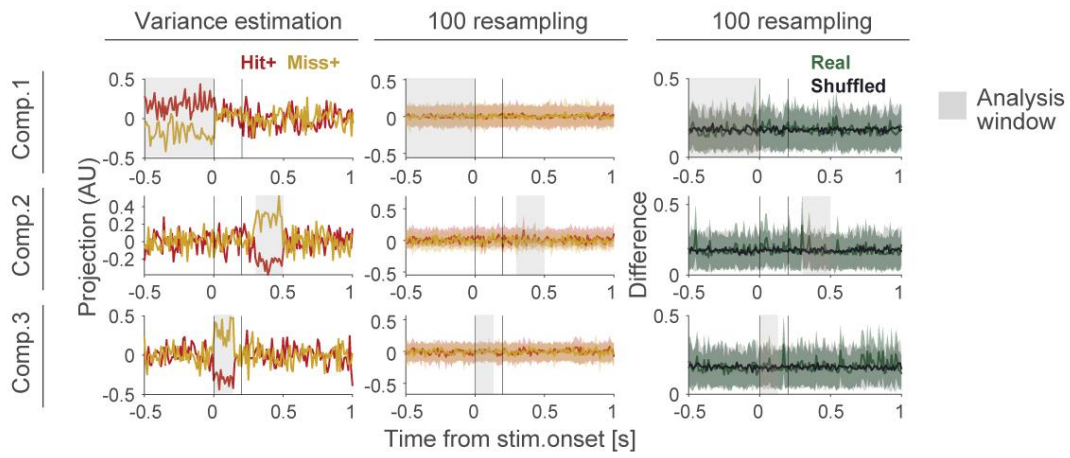
Figure.21 | State space analysis of the simulated dataset

The projections of each orthogonal axis were dissociated in mean population dynamics using all trials (left column), but its dissociations were completely diminished in resampling dataset applying training-estimation split methods (see methods). The shaded area indicates SD.
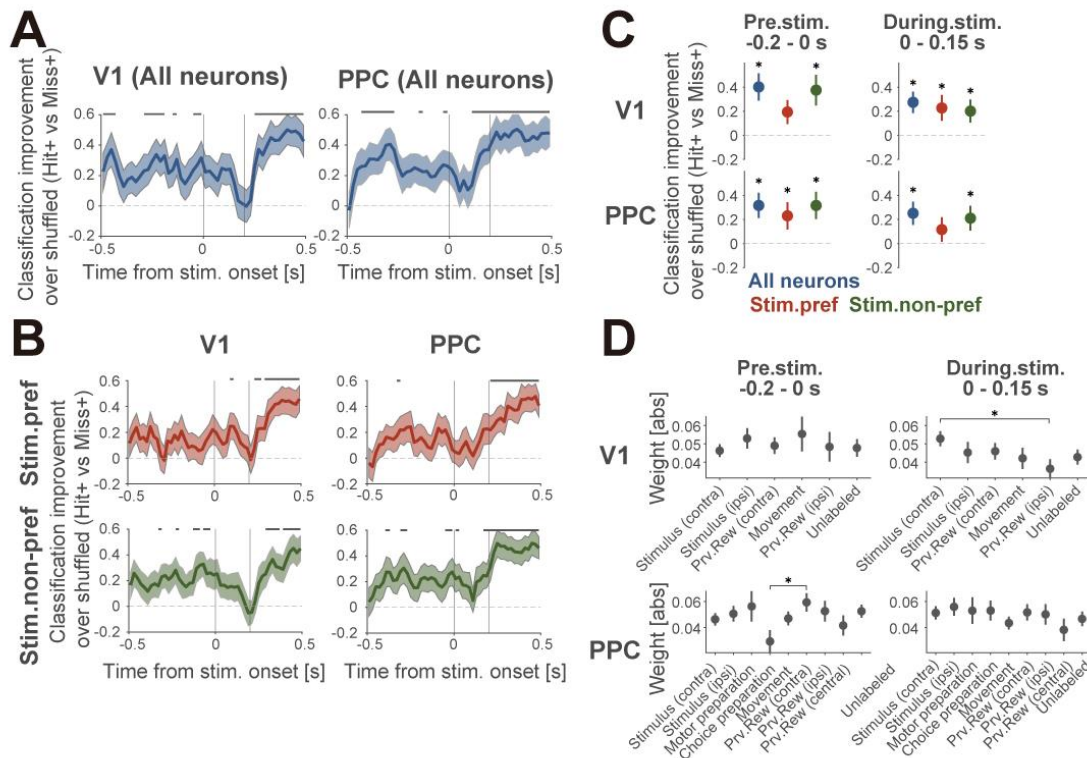
Figure.22 | Predictability of distinct choice type in V1 and PPC

(A) Classification improvement (real - shuffled classification accuracy) of classifiers trained by

all neurons in V1 (left) and PPC (right) in each time bin. The classifiers were independently

trained in each time bin. Shaded area shows SD. (B) Same as in (A), but each classifier trained

by stimulus-preferring (left) or non-preferring neurons (right) in V1 (top) and PPC (bottom). (C)

Classification improvement in pre-stimulus epoch (-0.2 to 0 s from stimulus onset) and during

stimulus (0–0.15 s from stimulus onset) for each population type. Error bars show SD. *p < 0.05;

mean ± 2SD > 0. (D) Absolute weight value for different neuron types in classifiers trained on all

neurons for each epoch. Neuron types were defined based on GLM analysis as depicted in Figures

8B and 8D except that the non-sensory neurons (e.g., prev. outcome, movement, etc.) here did not

include stimulus neurons (ipsi and contra). Only neuron types with >5% of the total number of

neurons are displayed. Data represent mean ± SEM. $*p < 0.05$; one-way ANOVA followed by
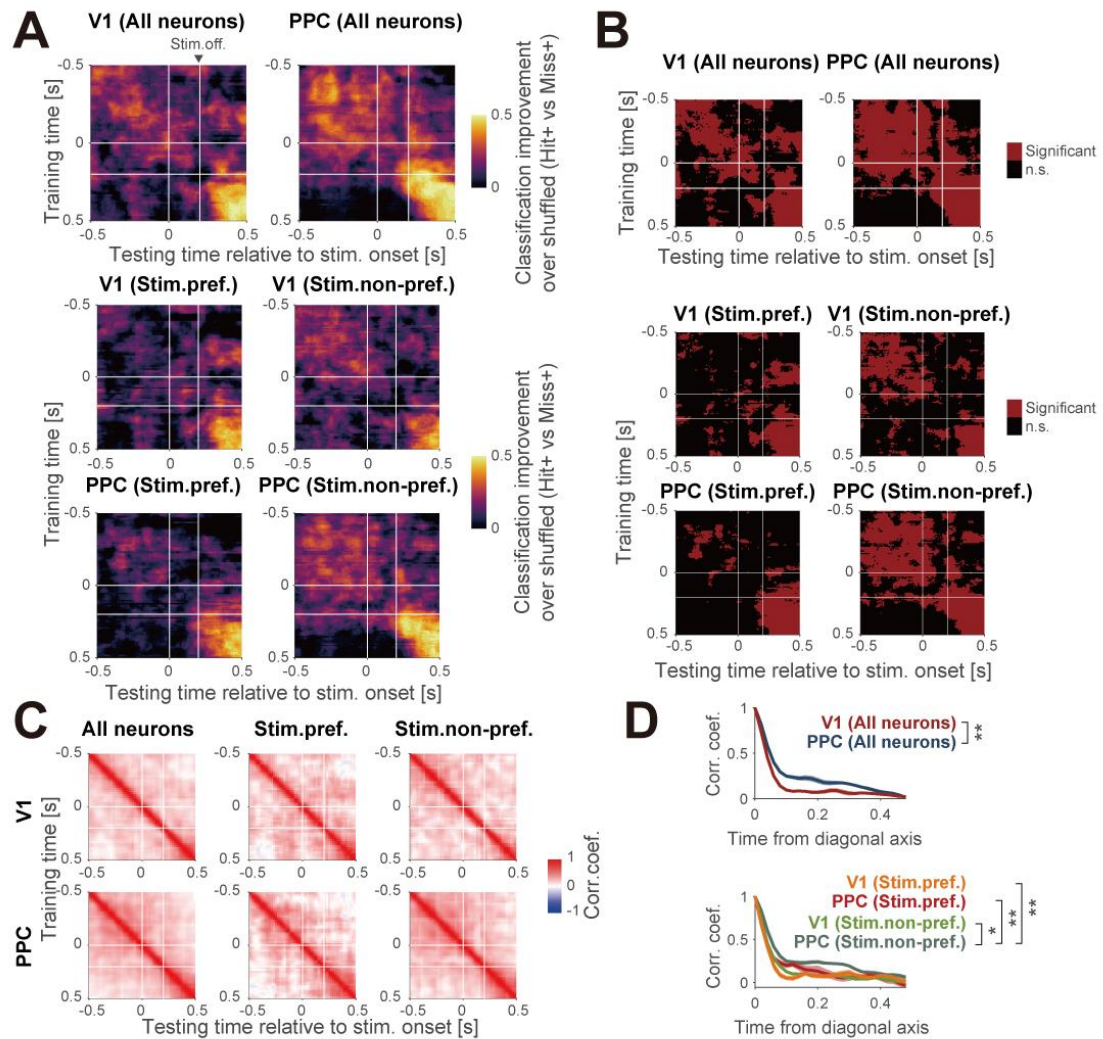
post hoc LSD tests.

Figure.23 | Time-varying classification performance and weight correlation

(A) Classification improvement computed from classifiers for each pair of training/testing time

points for all neurons, stimulus preferring, and non-preferring populations in V1 and PPC. (B)

Significant classification improvement maps corresponding to A. Red indicates a classification

improvement significantly above chance level (Mean – 2SD > 0). (C) Weight correlation of

classifiers for each pair of training/testing time points for all neurons, stimulus preferring, and

non-preferring populations in V1 and PPC. D, Time-varying correlation coefficients in all neurons

(top) and sub-populations (bottom). Shaded area indicates SEM. *p<0.05, **p<0.01, Kruskal-

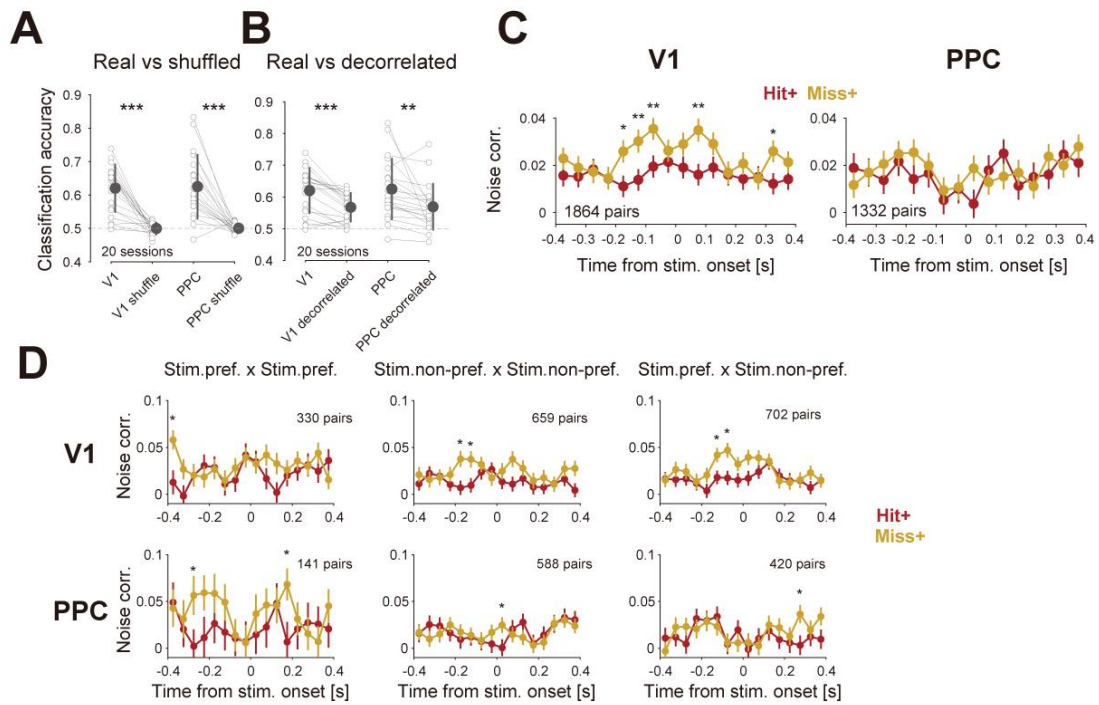Wallis test followed by post-hoc Tukey test for comparison. tests.

Figure.24 | Noise correlation in Miss+ trials increased around stimulus presentation in V1

(A) Classification accuracy for real and shuffled populations in each session in V1 and PPC. ***p

< 0.001 in V1; paired t test. (B) Classification accuracy for the real and de-correlated population

in each session in V1 and PPC. **p < 0.01; ***p < 0.001; paired t test. (C) Mean noise correlation

in each time epoch in V1 and PPC. The error bars show SEM. *p < 0.05; **p < 0.01; t test. (D)

Mean noise correlation in each time epoch with different neuron type combinations in V1 and PC.
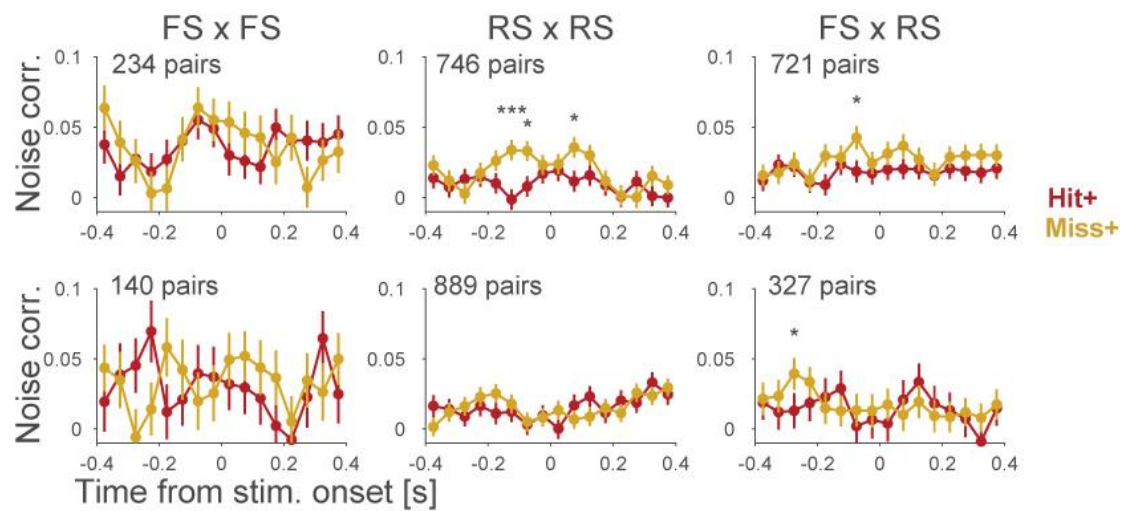
*p < 0.05; paired t test.

Figure.25 | Noise correlation in each cell-type

Mean noise correlation in each cell type pairs. Error bars show SEM. *p<0.05, ***p<0.001, t-test.

7   Appendix

7.1 Internal factor

Internal factor is a scientific term generally used in psychology and neuroscience, also called 'internal state'. Accumulating evidence of behavioral experiments indicates that our behavioral strategy and decision making is often fluctuated by our conditions, such as hunger, fatigue, satiety, and the other subjective aspects of our mind. These internally generated factors are examples of internal factors.

7.2 Narrow-spiking neuron

Cortical microcircuits are composed of neuron types with firing properties. In cortical neurons, two types of firing patterns were historically studied; broad waveform regular spiking (RS) and narrow waveform narrow spiking (NS) neuron (also called a fast-spiking neuron). These neurons are putatively thought of as excitatory and inhibitory neurons, respectively.

7.3 Support vector machine (SVM)

Support vector machine (SVM) is one of the machine learning algorithms to classify the category from a large dataset. The objective of the SVM is to find the hyperplane in the high-

dimensional data space (dimension corresponds to each data feature) that is optimally

classification between the different categorical data points.

7.4 Arousal

Arousal is often defined as the psychological and physiological state of awakening of sense

organs.